POLITECNICO DI TORINO

Master Course in Aerospace Engineering

Master's Degree Thesis

Testing of innovative sensors for implementation of prognostic techniques in aerospace environment

Supervisor:
Prof. Paolo Maggiore

Co-Supervisors:
Ing. Matteo Dalla Vedova
Prof. Daniele Milanese
Prof. Davide Luca Janner

Candidate:
Luigi Ricca

A.A. 2017/2018

Vorrei ringraziare il relatore e i corelatori che mi hanno seguito; in particolare il Professor Maggiore e l'Ingegner Dalla Vedova.
Grazie alla mia famiglia, ad Alessia e ai miei amici; un grazie speciale ad Alessia che mi è stata vicina per questi anni condividendo con me bellissimi momenti e permettendomi di superare i periodi di difficoltà.
Grazie ai miei genitori che, con supporto morale e sacrifici economici, mi hanno permesso di studiare e portare a conclusione questa laurea.

Abstract

This thesis is developed at the Mechanical and Aerospace Engineering Department (DIMEAS) of the Politecnico di Torino with the collaboration of Istituto Superiore Mario Boella and Potonext centre.

This work is related to the study of an innovative type of sensors integrated into the optical fibers; the peculiarity of being manufactured directly into the optical fiber gives the sensors good suitability for next-generation application.

These relevant features are linked to the dimension of sensors (they are lighter and smaller respect of the classic ones), to the immunity to electromagnetic fields and harsh environment, to the usability in explosive environment (since they make use of the light rather than electricity to carry information), to the possibility of multiplexing them on a single optical fiber (to increase the amount of useful information) reducing even more the total weight. All these properties make possible the development of new diagnostic and prognostic techniques to make more efficient the maintenance and reduce the time needed for it.

The objectives of this thesis are the development of a proper test bench to perform thermal tests, calibrate the FBG respect of temperature change, perform thermal compensation tests to see if the results have a sufficient accuracy.

The work made, and so the thesis, is subdivided into different phases; in a first phase is developed the test bench to achieve repeatable results with the lower external disturbance as possible, is take into account also the need of placing a tensioned fiber. This phase starts with a layout designed by the persons who worked on the strain measurements; the design is then changed different times to eliminate step by step the different source of errors; identified the correct layout thermal tests are performed to understand how the FBG is reacting at temperature changes in not ideal conditions.

Once a good familiarity on the behaviour of the FBG respect of the temperature changes has been taken, are performed thermal compensation tests to see if the results obtained have the sufficient accuracy needed for real-life applications.

Sommario

Questa tesi è sviluppata presso il Dipartimento di Ingegneria Meccanica e Aerospaziale del Politecnico di Torino (DIMEAS) in collaborazione con l'Istituto Superiore Mario Boella e il centro Photonext.
Questo lavoro è relativo allo studio di un tipo innovativo di sensori integrati direttamente all'interno delle fibre ottiche; la peculiarità di essere costruiti nella fibra li rende adeguati all'utilizzo in applicazioni di nuova generazione.
Queste importanti proprietà sono legate alla dimensione dei sensori (sono più leggeri e piccoli rispetto a quelli convenzionali), all'immunità rispetto a campi elettromagnetici e ambienti aggressivi, alla possibilità di utilizzo in ambiente esplosivo (poiché utilizzano la luce piuttosto che l'elettricità per il trasferimento di informazioni), alla possibilità di inserire dozzine di sensori in un'unica fibra (per incrementare la quantità di dati prelevati) riducendo ulteriormente il peso. Tutte queste proprietà rendono possibile lo sviluppo di nuove tecniche prognostiche e diagnostiche per rendere la manutenzione più efficiente e ridurre il tempo impiegato per portarla a termine.
Gli obiettivi di questa tesi sono lo sviluppo di un banco prova per eseguire i test termici, calibrare il FBG riguardo la variazione di temperatura, eseguire test di compensazione termica per vedere se i risultati ottenuti hanno una accuratezza sufficiente.
Il lavoro svolto, e di conseguenza la tesi, è suddiviso in differenti fasi; in una prima fase è stato sviluppato un banco prova per ottenere risultati ripetibili e influenzati il meno possibile da fattori esterni, è stata presa in considerazione anche la necessità di inserire una fibra tensionata. Questa fase parte da una configurazione studiata dai tesisti che si sono occupati delle analisi di deformazione; il progetto è quindi cambiato diverse volte per eliminare passo dopo passo le differenti fonti di errore; identificata la corretta configurazione sono stati eseguiti dei test termici per analizzare il comportamento del FBG a variazioni di temperatura in casi non ideali.
Acquisita una buona familiarità riguardo alla risposta del FBG alla variazione di temperatura, sono stati eseguiti dei test di compensazione termica per vedere se i risultati ottenuti presentano una accuratezza sufficiente all'impiego in applicazioni reali.

Table of contents

List of figures

List of tables

1 Introduction

Optical fibers are becoming increasingly important in many disciplines thanks to their characteristics, in fact optical fibers are able to transmit information across long distances with low loses and with a high bitrate [1]; furthermore optical fibers are also lighter and thinner compared to the normal copper cables thus resulting in a decreasing of the mass, objective always wanted especially in the aeronautical and space fields.

As you can guess from the suffix optical, the way the information are send is by the light and not by the electricity, this makes them immune to electromagnetic interference; moreover the fiber is made with silica that is resistant to temperature and to harsh environment [1] allowing, therefore, to use them in places where was impossible to use copper cables like the interior of an electric engine.

In addition, the fiber could also be used as a sensor, there are different ways we can create a sensor, but the way chosen exploits the Fiber Bragg Grating principles, these sensors are able to identify variations in stress, temperature, pressure without the need for an electrical supply; an important peculiarity of these kinds of sensors is that the FBG is imprinted on the optical fiber itself so has the same characteristic and strength of the silica fiber.

All these characteristics, plus the possibility to put a set of FBG on a single fiber, bring the fibers to acquire a great importance in the aerospace fields, in particular in the prognostic applications, area in which there is a need for a large amount of data to better know and predict what the system is doing and what will do.

The fact that the data obtained from a single FBG are affected by all these elements: temperature and strain in particular; involves that a particular procedure is identified to separate the contribution of one physical entity from the other.

1.1 Objectives

The main goals of this thesis are the identification of an optimum packaging of the fibers to be used as strain and temperature sensors in future projects, the calibration of the FBG respect of temperature changes and the performing of thermal compensation tests to see if this compensation is usable in real life devices; the optimum solution must include a proper locking system and a proper locking geometry to have a packaging easy to set up obtaining also accurate and precise measurements.
To be sure that the solution found is enough precise and accurate it will be necessary to build a test bench and design proper facilities to calibrate the sensors, these facilities should be again easy to sets up and give adequate confidence on the results obtained.
In order to reach this goal the thesis will focus in a first time on the calibration of the optical fiber to sense the temperature changes of the desired object; in a second time it will be performed the so-called Thermal Compensation, that is the use of a second fiber to correct the shift induced by the variation of temperature on a first fiber used to measure the stress on the desired object.

1.2 Thesis structure

This thesis is subdivided into the following sections:

- Theoretical discussion of the FBG working principles.
- Test bench design.
- Results of the thermal tests.
- Results of the thermal compensation tests.
- Conclusions
- Appendix

The theoretical discussion presents the main equations that characterise the FBG working principles; in the test bench design chapter is presented the process followed to design a proper test bench with all the steps and the main problems that lead to the change of the

design, this chapter is not subdivided into thermal analysis and thermal compensation because the test bench designed for the first case is used also for the second one.

In the results chapter are reported the results obtained in the different tests with highlighted the problems that lead to the design change; finally, in the concluding chapter are summarised the most important results obtained.

Is present also an appendix where is presented a mathematical system to simulate the response of the real system when a temperature change is imposed.

2 Optical fiber and sensors

Optical fibers are becoming an important element in the technological research for applications which so far have been closed due to the limitations of the materials used; the fibers, and in particular the sensors built thanks to the fiber, or in the fiber itself, allow to overcome these limitations opening new windows on fields and applications impossible to travel before.

2.1 Optical fiber description

Optical fibers are devices made of plastic or silica depending on the performance desired: the plastic optical fibers are less expensive but present a greater attenuation, they are used mainly in applications where the low cost is important and the light is guided across short distances. The silica optical fibers are more expensive but with also higher performances, the attenuation is lower and they are more resistant to harsh environment; these kinds of fibers are used where the main goal is the performances and cost increase is in the second level.

2.1.1 Optical fiber structure

The optical fiber is composed of a series of layers shown in Figure 2.1:

- Core.
- Cladding
- Coating.

The core is the central element involved in the transportation of the light thanks to the total reflection phenomena. The cladding is a silica or plastic layer where the refractive index is lower respect of the index of the core permitting the total reflection. The coating is a protective layer to increase the mechanical characteristics.

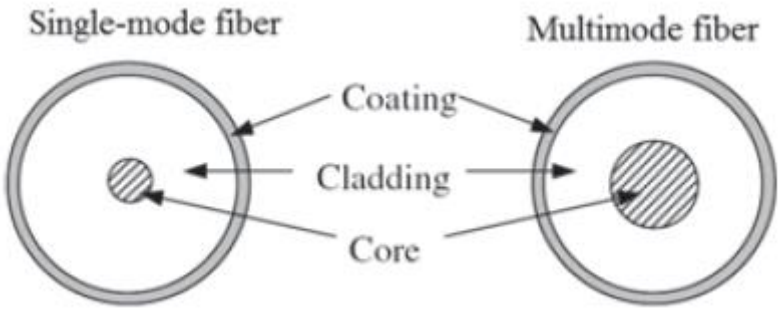

Figure 2.1: section of two fibers showing the main elements and the main differences (from [2])

The optical fibers are divided into two main categories:

- Single-mode fibers.
- Multi-mode fibers.

The main difference is the core diameter and the consequent number of modes that the fiber is able to carry; a single-mode fiber is able to carry only a single mode and so also the power transmitted is lower; the multi-mode fiber has a higher numerical aperture permitting to transmit more power, but the modal dispersion degrades the data transmitted allowing the use of this fiber only on short distances; this problem is shown in Figure 2.2.

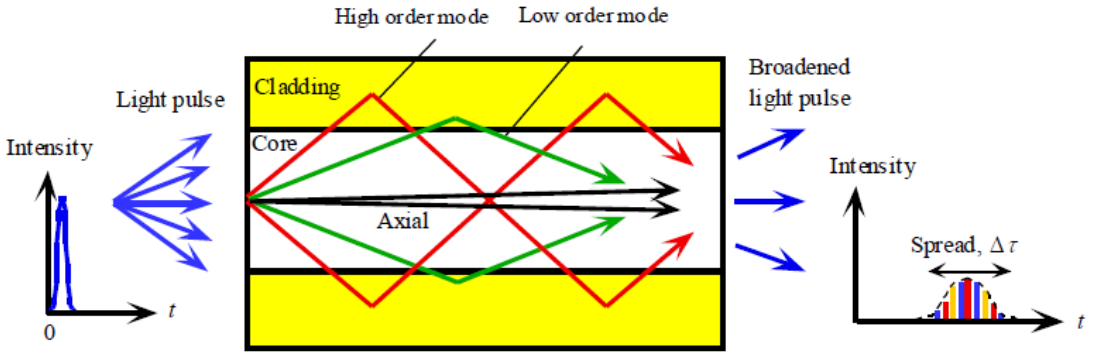

Figure 2.2: multi-mode fiber with modal dispersion

The dimension of the core of a single-mode fiber is about 10 μm, the core of a multi-mode one instead is between 50 and 100 μm [2]; the dimension of the cladding is a standard value and is 125 μm. The fibers used for this thesis are the single-mode type with a polyimide coating.

2.1.2 Optical fiber theory

The optical fiber is able to transmit the light across long distances with low losses thanks to the total internal reflection; this is a phenomenon that presents when the core has a higher refractive index respect of the cladding and the light is injected into the fiber with a particular angle higher than the critical angle.

The total internal reflection refers to the Snell's law reported in equation (2.1):

$$n_1 \sin \alpha_i = n_2 \sin \alpha_r \tag{2.1}$$

Where n_1 and n_2 are the refractive indexes of the two elements, α_i is the incidence angle and α_r is the refraction angle as visible in Figure 2.3 where $n_1 > n_2$.

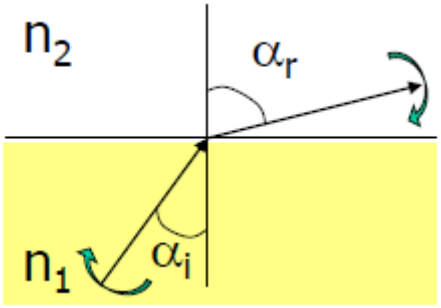

Figure 2.3: Snell's law graphical representation

The consequence of this equation is that is possible to find an incidence angle for which the refraction angle is 90°, so the radiation is fully confined into the core; to find this angle it is possible to solve the equation (2.2):

$$\alpha_{i0} = \arcsin \frac{n_2}{n_1} \tag{2.2}$$

In the case of optical fibers the light beam is injected from a third medium, so it must be considered the initial refraction that is present between this third medium and the core to calculate properly the right injection angle to obtain the total internal reflection.

First of all, it must be considered the refraction between the first element and the core, this is shown in the following equation:

$$n_0 \sin \alpha = n_1 \sin \left(\frac{\pi}{2} - \vartheta_c\right) \tag{2.3}$$

To have the total internal reflection must be verified the equation:

$$n_1 \sin \vartheta_c = n_2 \sin \frac{\pi}{2} \tag{2.4}$$

Replacing ϑ_c it is obtained the final equation:

$$\sin \alpha_{max} = \frac{\sqrt{n_1^2 - n_2^2}}{n_0} \tag{2.5}$$

The coefficient $\sqrt{n_1^2 - n_2^2}$ is called Numerical Aperture and so the equation could be re-written as:

$$\sin \alpha_{max} = \frac{NA}{n_0} \tag{2.6}$$

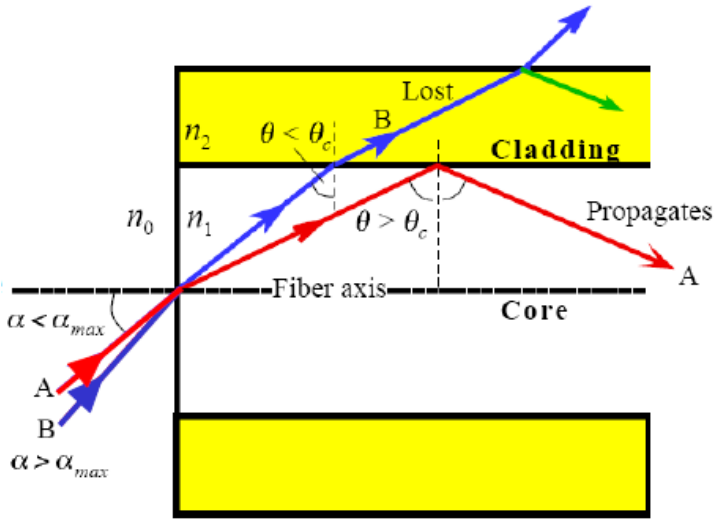

Figure 2.4: total internal reflection angles considering also the outside medium

2.2 Optical fiber sensors

A great advantage to using the optical fiber in today's applications is the possibility to build a sensor directly into the fiber itself; the mechanism by which optical fibers can work like sensors can be one of these four different ways [2]:

- Intensity modulation: is used the change of light intensity to take information.

- Polarisation modulation: external actions on the fiber could mix two different polarisations that, on the contrary, would remain distinct.
- Phase modulation: is used the difference in the phase, so in the arrival time, of the input caused by external deformations.
- Spectral modulation: the mechanical or thermal strain produce a shift of the wavelength reflected.

For the project presented in this thesis are used spectral modulation sensors called Fiber Bragg Gratings or FBG.

2.2.1 Fiber Bragg Grating theory

An FBG is an intrinsic sensor based on a periodical modulation of the refractive index of the core of the fiber; it is photo-imprinted in the fiber thanks to the photosensitivity of this one. The Germanium is used in the core to raise the value of the refractive index and, when is exposed to UV light, increase even more this value [3], so the grating is printed using this kind of light in two main different ways: it can be used a single UV beam and a mask to create darker and brighter areas and change accordingly the refractive index, another way is the use of two distinct UV beams to create an interference pattern on the fiber [4].
Regardless of the way used the result is a change in the refractive index that works like a selective mirror and reflects a particular wavelength, this wavelength, called Bragg wavelength, is given by the equation:

$$\lambda_B = 2n\Lambda_{\mathrm{G}} \tag{2.7}$$

Where:

- λ_B is the wavelength reflected by the FBG.
- n is the refractive index of the fiber.
- Λ_G is the pitch of the grating as shown in Figure 2.5.

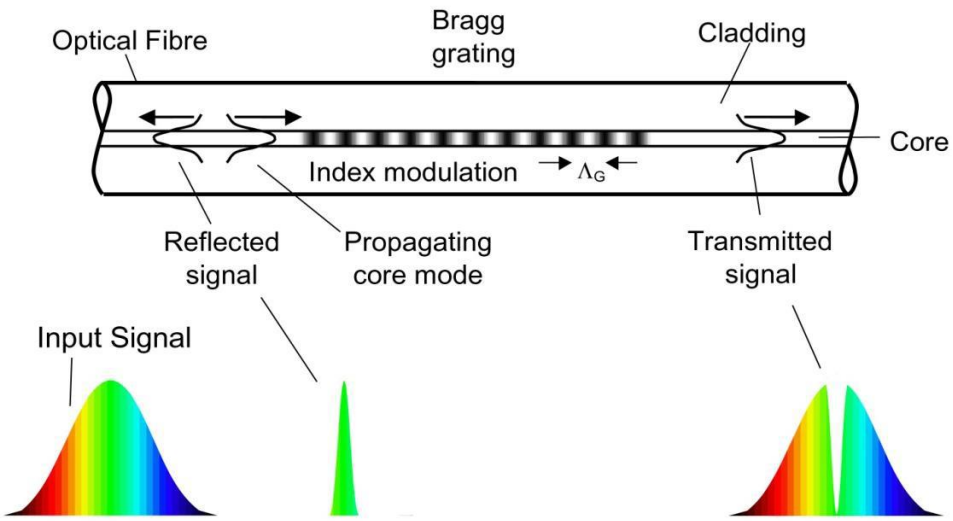

Figure 2.5: schematic diagram of an FBG having an index modulation of spacing Λ_G inside a single-mode optical fiber [3]

The wavelength reflected by the FBG is affected by two different main factors: the change of the pitch of the gating caused by a deformation, both mechanical and thermal; and the change of the refractive index caused by the temperature variation. The shift in wavelength is described by the equation (2.8):

$$\Delta\lambda_B = \lambda_B(1 - p_E)\Delta\varepsilon + \lambda_B(\alpha_\Lambda + \alpha_n)\Delta T \tag{2.8}$$

Where:

- p_E is the strain-optic coefficient, for optical fiber is around 0,22 [4].
- α_Λ is the thermal expansion coefficient, for silica α_Λ = 0,5 x 10^{-6} °C^{-1}.
- α_n is the thermo-optic coefficient.
- $\Delta\varepsilon$ is the variation in deformation expressed in $\mu\varepsilon = 10^{-6}\varepsilon$.
- ΔT is the variation in temperature expressed in °C.

The thermo-optic coefficient can be written according to the equation

$$\alpha_n = \frac{dn_0}{dT}\frac{1}{n_0} \tag{2.9}$$

With n_0 that is the effective refractive index of the optical fiber, dn_0/dT is the change of this index caused by the change in temperature; for optical fibers common values are:

- n_0 = 1,4575 [5].

- dn_0/dT = 1,2 x 10^{-5} °C^{-1} [5].

The equation (2.8) can be rewritten in an easier way to be used in experimental tests because the contributions given by the two terms on the thermal part can't be distinguished; it comes to:

$$\Delta\lambda_B = K_\varepsilon \Delta\varepsilon + K_T \Delta T \tag{2.10}$$

The tests made in the thermal analysis section are aimed to find the parameter K_T for the particular fiber used in the particular setup analysed; for the fiber used with the interrogator, referring to equation (2.8) and (2.9), this parameter can range from 0,0133 nm/°C to 0,0137 nm/°C.

The value of thermo-optic coefficient changes slightly from a fiber to another, in equation (2.11) and equation (2.12) is reported another way to calculate the change of the refractive index in function of temperature in °C [6]; using these the result the value of K_T ranges from 0.0093 nm/°C to 0.0096 nm/°C.

A result between these two extreme values could be acceptable.

$$n_{eff} = n_0(1 + 5{,}327 \times 10^{-6}T + 4{,}773 \times 10^{-9}T^2 - 1{,}391 \times 10^{-12}T^3) \tag{2.11}$$

$$\frac{dn_{eff}}{dT} = 7{,}764 \times 10^{-6} + 1{,}391 \times 10^{-8}T - 6{,}082 \times 10^{-12}T^2 \tag{2.12}$$

$$\alpha_n = \frac{dn_{eff}}{dT}\frac{1}{n_0} \tag{2.13}$$

3 Test bench design

In this chapter is explained the design of the test bench used for the measurements in the different tests, the chapter is not subdivided into Thermal Analysis and Thermal Compensation sections because they are closely related to each other.
The test bench is fundamental for the analysis of the FBG response to be sure that the data taken are not affected by external disturbances; with the effects of external factors the results could be deeply affected by errors and so the conclusions drawn could be completely or partially wrong.
As it will be seen all the changes made to the different projects are aimed to obtain a reading of the data without such errors and with a deep knowledge about what is that the sensors are actually sensing.
The aim of the test bench is to warm and cool the fiber and sense the variation of wavelength thanks to an interrogator and bind this shift to the temperature taken with a proper sensor; in a second time it will also be requested to design a system to change the strain of the fiber while is changing the temperature to conduct the tests about thermal compensation; the main and indispensable elements of the test bench will be:

- Peltier cell: heat source.
- PT100: temperature sensor.
- Optical fiber with FBG.
- Microcontroller.
- Interrogator.

The main difficulty of the setup is the certainty that the temperature measured by the FBG is the same measured by the PT100, this difficulty will be the main reason for the changing of the design.

3.1 Vibration isolation system

An important first source of external disturbances are the vibrations; the laboratory is placed near the street where there is the passage of trams and other heavy transport vehicles; in tests conducted before this thesis was shown that the vibrations produced by these vehicles affect the results introducing errors.

All the elements used for the tests are placed on a damping system composed of two layers: a first layer is a heavy breadboard with damping properties, the second layer is an optical table with rubber dampener and rubber air pockets; this two-layer system isolates all the devices used for the tests from external vibrations.

Figure 3.1: breadboard used for the assembly of the test bench

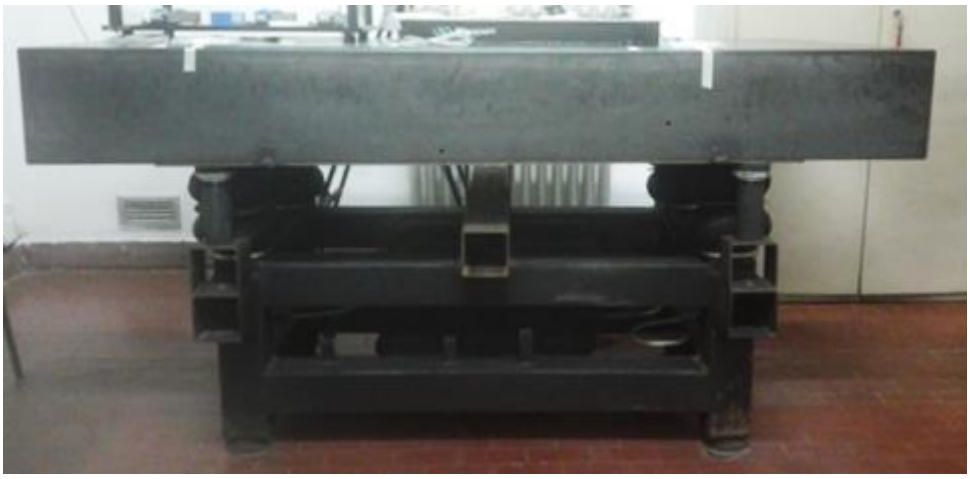

Figure 3.2: optical table with rubber dampeners

3.2 Microcontroller

The Peltier cell is powered through the microcontroller TEC-1091 made by Meerstetter Engineering, it uses a closed-loop system with a PID controller to set de desired characteristic of the response; the loop is closed thanks to the PT100 sensor.
The TEC-1091 doesn't drain the needed current directly from the electricity network, but this is provided by a power supply with limitation in volt and ampere to avoid an excessive power drain; when the power required is too high the supplier disconnects the microcontroller to avoid overheating and possible damages.

Figure 3.3: TEC-1091 microcontroller

In Figure 3.4 is shown a schematic representation of the microcontroller with the main connection to the external devices with the required polarity; it is required to be very careful to connect the different cables with the correct polarity to avoid damaging the microcontroller or having incorrect readings of the sensor.
The PID requires a careful tuning to obtain the desired performance; after a lot of tests two sets of tuning parameters have been identified, the first one for a steady and continuous increase of the temperature, but with low capability in maintaining a defined value; the second one is optimized to reach and maintain thea desired temperature, but the transition between two values presents a lot of oscillations and is not constant.

Below are shown the parameters to be used depending on the desired response; to have a consant change of the temperature the values are:

- Coarse temp ramp: 0,02 °C/s
- Proximity width: 1 °C
- Kp: 30 %/°C
- Ti: 10000s
- Td: 0s

To have a good capability to reach and maintain a desired temperature the parameters values are:

- Coarse temp ramp: 1 °C/s
- Proximity width: 0,1 °C
- Kp: 80 %/°C
- Ti: 20s
- Td: 6s

The values reported, especially those for maintaining a desired temperature, are referred to the thermodynamic system described in chapter 3.6 and chapter 3.7.

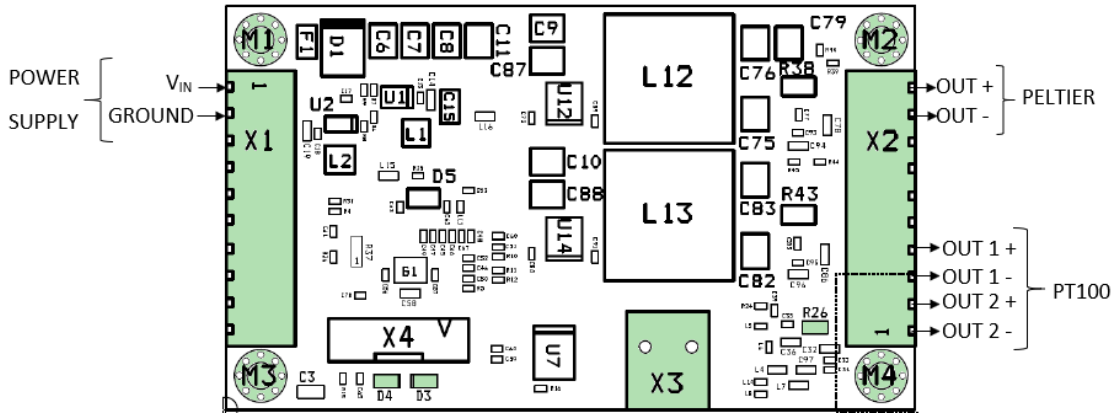

Figure 3.4: microcontroller schematic with the main connection with power supply, Peltier and PT100 (TEC-1091 Datasheet)

The tuning of the PID is made using the so-called "good gain method", this procedure consists in finding a value of a pure proportional controller able to create an overshoot and a little undershoot; then this value is used to find also the other coefficients of the controller; in particular the steps to be followed in order to tune correctly the PID are [7]:

- In manual mode bring the system near the operational point.
- Set $T_i = 10000$ (the maximum possible in the software) and the $T_d = 0$ to be sure that the controller is a pure proportional.
- Increase the K_P to K_{PGG}, the so-called good gain proportional value, this is the value for which the system presents an overshoot followed by a little undershoot.
- Note down the time between the overshoot and the overshoot (T_{OU}), this is the starting parameter for the integrative term, the value of the integrative coefficient could be found using the equation: $T_i = 1{,}5\ T_{OU}$.
- The introduction of the integrative term will reduce the stability of the system, so the new proportional parameter is: $K_P = 0{,}8\ K_{PGG}$.
- If the controlled system presents some fluctuation a derivative term is needed, the value of this therm is found via an iterative mode taking into account the possibility of introducing instability if is present some noise in the PT100 signal.

3.3 FBG interrogator

The tensional status and the temperature of the FBG is read thanks to sending a laser beam in the fiber and analysing the wavelength of the feedback; all these things are made by the interrogator of the Smart Fibers. This interrogator, called SmartScan, is a compact hardware able to send a laser beam and analyse the returning signal, the data obtained about the reflected wavelength could be displayed on the computer screen or could be saved in a .log file, this file could then be opened in a Matlab project to process the raw data.

The SmartScan is also able to perform a first processing of the raw data reporting the value of the temperature or pressure based on the type of sensor selected and the characteristic of the FBG; this interrogator has four input for four different optical fibers and 16 possible FBGs per fiber, so the total amount of FBGs that could be used together is 64; the fibers used must have a Bragg wavelength from 1528 nm to 1568 nm.

Figure 3.5: SmartFibers interrogator used for the tests

3.4 First configuration, aluminium blocks

The first project is shown in Figure 3.6 and it includes a system of three aluminium blocks to warm or cool uniformly the fiber and the PT100; it was chosen aluminium in order to have a good thermal conductivity to bring the fiber and the PT100 at the same temperature and to have thermal sinks for the Peltier.

The first element shown in Figure 3.7 is the base to host the Peltier, it works as a heat sink; in Figure 3.8 is visible the base for the fiber, this element is placed between the Peltier and the fiber so the heat can be distributed on a higher surface, is present a groove

of 0,1 mm that is needed to not crush the fiber; the Figure 3.9 shows the third block with the housing for the PT100, this temperature sensor is glued with an elastic and thermoresistant silicon. These three pieces are positioned on the breadboard thanks to four threaded bars and eight bolts.

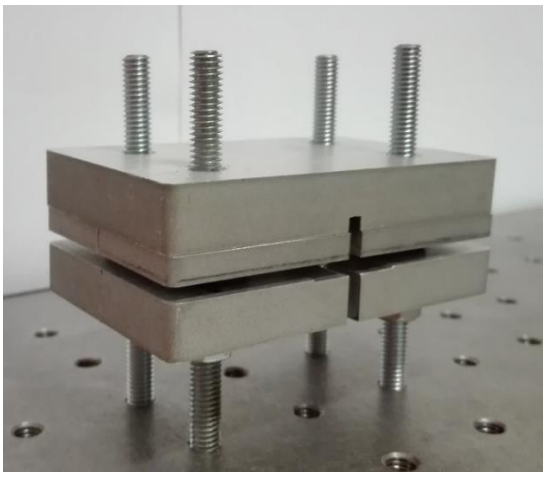

Figure 3.6: first setup fully mounted, are visible the three different layers of aluminium

Figure 3.7: Peltier cell base

Figure 3.8: optical fiber base

Figure 3.9: PT100 base

This kind of layout was chosen to have a uniform temperature around the fiber and the PT100 but the Peltier used, the RS 490-1250, with only 5 W of power is unable to warm the optical fiber base, the difference between the actual temperature and the one desired leads to an increase of the error, so the PID controller demands too much current and the power supply shuts off.

The layout used for the first series of tests is shown in Figure 3.10 and is similar to the one just explained but with the removal of the optical fiber base, now the PT100 and the Peltier are in contact and the fiber is put between these two elements.

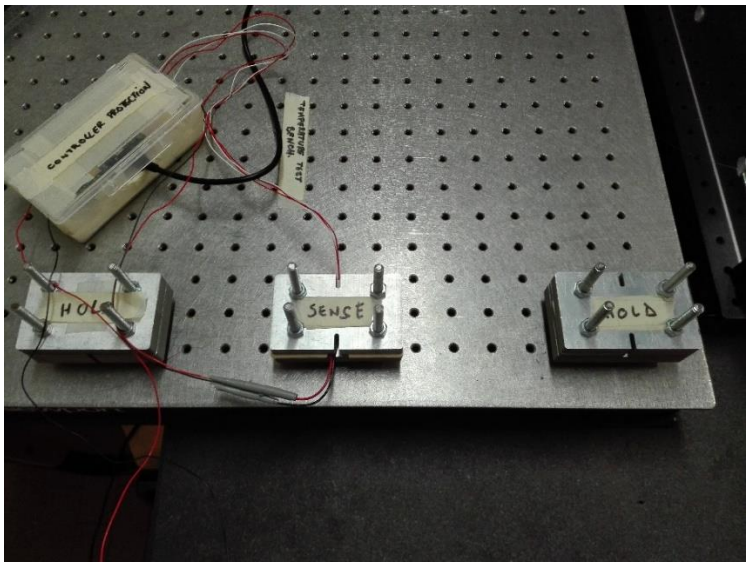

Figure 3.10: layout for the first series of tests

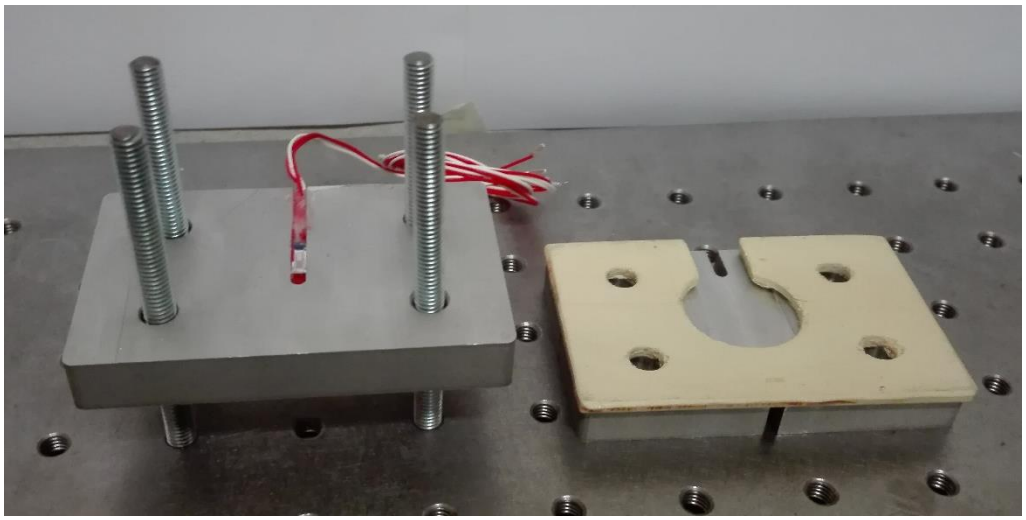

Figure 3.11: Assembly opened for best understanding

In Figure 3.11 the full assembly is opened for a better understanding, on the right is visible the Peltier housing and a wooden sheet to isolate the hot and the cold side; on the left is in position the PT100 housing with the sensor glued in his hole. The fiber will be placed on the left block, the main difficulty in this configuration is that the FBG, the PT100 and the Peltier must be in the exact same place in order to be sure that the temperature measured by the FBG is the same measured by the PT100.
In the section 4.2.1 are reported the results obtained with this layout with the relative problems.

3.5 Second configuration, metal sheet

The second try to build a working test bench is focused on the reduction of thermal inertia by reducing the mass of the metal to be warmed and using plastic supports for insulation. The layout presents these different layers from bottom to top:

- Plastic base with metal sheet and PT100 glued under it as shown in Figure 3.12 and Figure 3.13.
- Optical fiber with the FBG.

- Metal sheet to spread the heat.
- Peltier.
- Metal block to be used as heat sink.

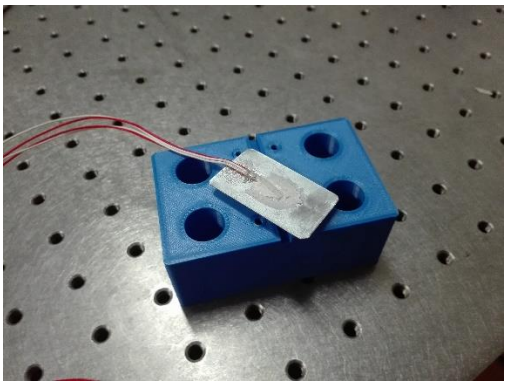

Figure 3.12: PT100 glued to the metal sheet

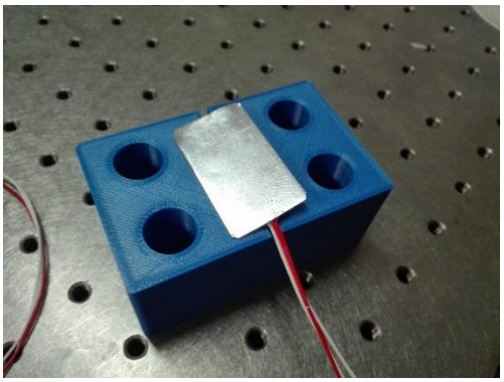

Figure 3.13: PT100 mounting configuration

The plastic base is the same used for the test on the strain with glued fiber, the hole made for the epoxy glue houses the PT100; the glue used is a thermal type to increase the heat transmission and reduce the warming time of the sensor.
In the section 4.2.2 the results are presented, again the problems about the uncertainty of the temperature that the PT100 is actually sensing leads to the modification of the design.

3.6 Third configuration, water system

The need to solve the problem about the uncertainty of the temperature that the PT100 is actually sensing leads to a new project; the idea is to use a water mass with inside the FBG and the PT100, both completely submerged. The Peltier warms the water and, thanks to its convective motions, we are sure that the PT100 is at the same temperature of the fiber.
This new project needs a new device able to host the Peltier, the water, and the PT100 and the FBG inside the water preventing to create small bending radius in the fiber; this new device is designed in CATIA V5 and then printed in 3D in PLA plastic. As shown in Figure 3.14 and Figure 3.15 the PLA block presents four holes to fasten it to the

breadboard, in the centre there is a square hole to host the water, the bottom of the hole is closed with the Peltier that in this way can warm the water on one side and is in contact with a heat sink, the breadboard itself, on the other side.

The Figure 3.16 shows the final setup with the temperature sensor and the FBG fully surrounded by the water, the fiber passes through the block thanks to a drilled hole.

This important change of the design introduces a problem in the system; the water does not warm or cool at the same speed of the Peltier and the PT100 is sensing the temperature of the water, not the one of Peltier, so this is a delay in the feedback loop; this delay leads to an increase in system instability and the software of the microcontroller must be tuned; the values presented in chapter 3.2 are found using the system of chapter 3.7, but are also useful for this configuration.

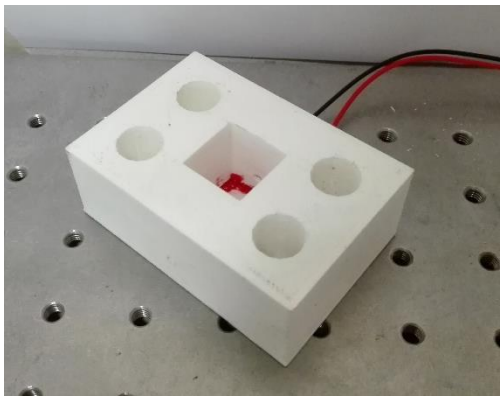

Figure 3.14: up side of device used

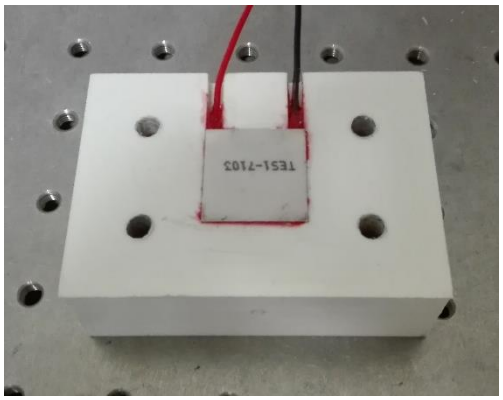

Figure 3.15: down side of the device with the Peltier

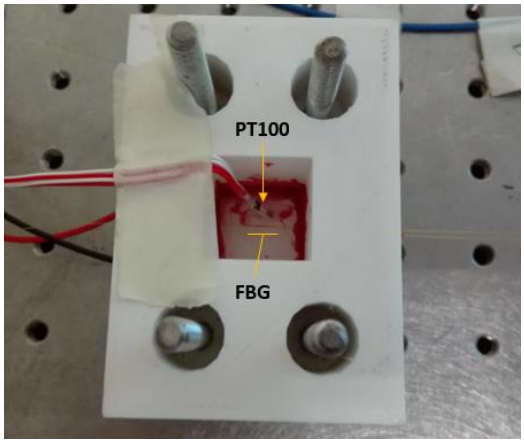

Figure 3.16: complete setup with the PT100 and the FBG in the water mass

3.7 Fourth configuration

This configuration is developed starting from the design explained in chapter 3.6; now the intention is to have two fibers: one completely free to move for the temperature measurements and one locked on a micrometre to apply some strain.
The design is changed because in the system used before the fiber is locked with silicone on both sides of the PLA block, so if strain is applied it is unknown the force that the silicone is exchanging with the fiber and there are some uncertainties about the strain that the FBG is actually measuring.
To keep all the advantages of the use of the water mass, but to have the fibers free to move a tilted configuration is developed; in Figure 3.17 is shown the Catia design of the water housing.

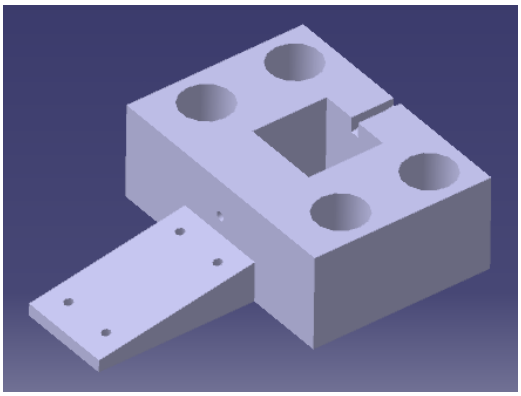

Figure 3.17: water housing with fiber locking base

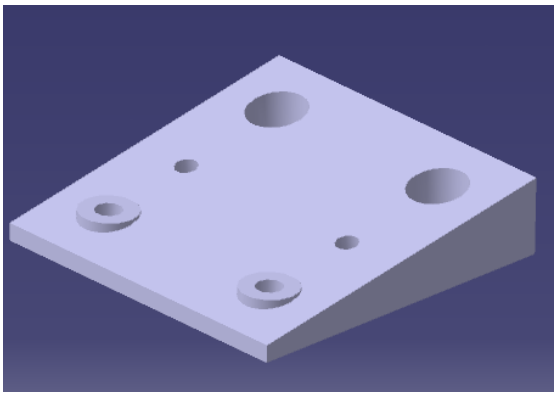

Figure 3.18: micrometre tilted base

The housing for the Peltier cell and the hole for the water are the same as before, but the big difference is the positioning of the fiber: as it is best visible in Figure 3.19 the hole and the groove made to allow the passage of the fiber are tilted and the angle is the same of the fiber locking base in order to position the fiber on a straight line; with this configuration, on the side of the micrometre the fiber exits the water without the need of the sealant. The silicon is instead needed on the other side, but because of the very small distance from the end of the hole and the Araldite locking system (less than 1 mm) it could be neglected the displacement of the glued section of the fiber, with a distance of

1 mm and a strain of 3000 με the displacement is only 0,003 mm; moreover when the silicone is applied the fiber could be moved slightly to detach the coating from the sealant, so the fiber could move more freely and the water does not come out.

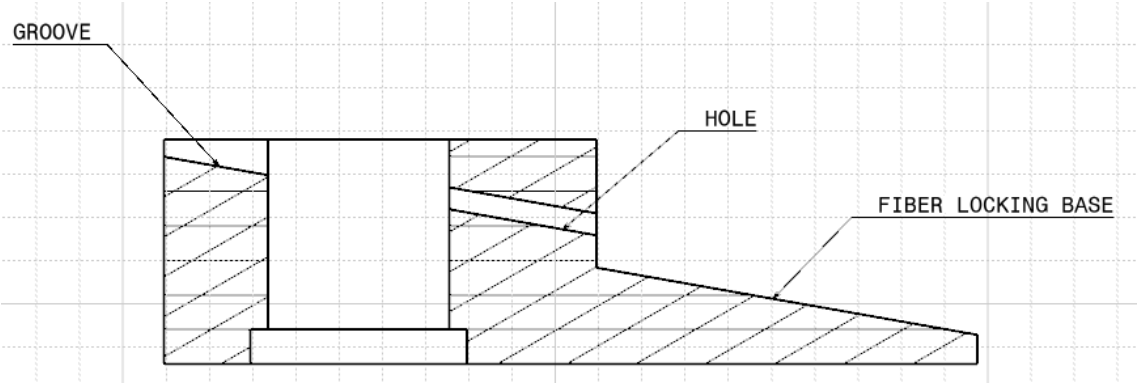

Figure 3.19: water housing and fiber base section

To prevent fiber from bending there is the need to maintain it on a straight line, so also the micrometre must be placed on a tilted base that is shown in Figure 3.18.

The first tests made on the response of the fiber at the temperature change at different level of tension shows a problem because the fiber is changing the wavelength even if both temperature and strain are steady; all are reported in 4.2.4.

The shift in wavelength with both temperature and strain steady is caused by the thermal deformation of the PLA when the water is heating, because of the base for the fiber locking system is directly connected with the water housing it moves back and induces further deformations in the fiber.

The design is therefore slightly changed to decouple the fiber locking system base from the water housing and so allow this last element to move freely under thermal expansion without affecting the FBG measurements.

In Figure 3.21 is visible a 3D render of the new base for the fiber locking system now separate from the water housing, it is necessary to increase the dimensions to implement four holes to fasten this element to the breadboard.

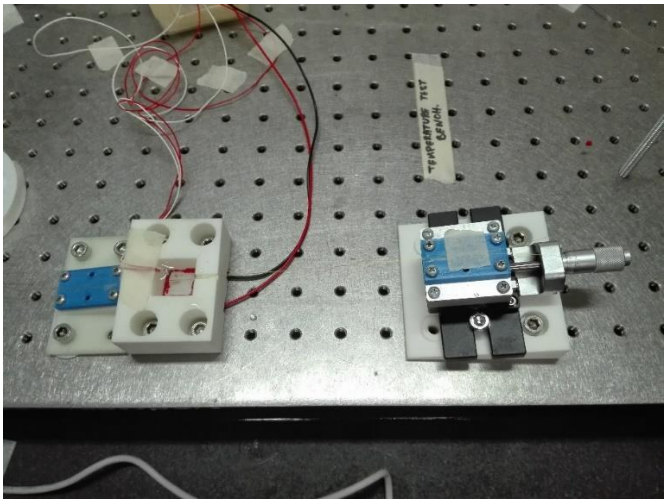

Figure 3.20: final setup

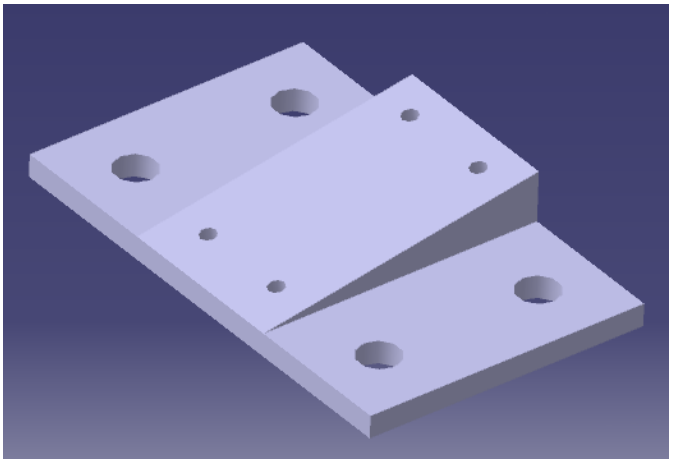

Figure 3.21: new design for fiber locking system

For the thermal compensation tests there is the need to use two different fibers: one for the measurement of the strain, affected also by temperature; and one for the measurement of the temperature only.

The second fiber must be free to move in order to not be affected by mechanical deformation; in this first test it is been decided to break the fiber after the FBG and insert it into the water, the fiber is locked only on the micrometre with an adhesive paper tape visible in Figure 3.20, in this way it can move freely; then the fiber passes through the

groove and the FBG is placed near the one used for strain measurement to be sure that the temperature sensed is the same.

4 Results

In this chapter are reported the results obtained thanks to the tests made and the problems encountered which led to the modification of the project; the data are taken in two ways: on an excel sheet reporting the wavelength at a certain temperature and via the log files made by the interrogator and the controller, these log files are then processed by a Matlab script.
There are two main sections: one that encloses the results obtained for the thermal analysis and another section that enclose the ones obtained for the thermal compensation.
The data for the thermal analysis are not taken using always the same logic because the change of design, explained in chapter 3, leads to a change in thermal capacity and so leads in a change of the time needed to the system to reach the right temperature; the time spent from a change in temperature to the next is adapted case by case.
Different is the case of thermal compensation where the system is brought to a defined temperature and then is performed the strain analysis with constant steps of 10 seconds at a steady strain and others 10 seconds to change the strain value.

4.1 Propagation of the measurement errors

Before the presentation of the results obtained during the tests made, is necessary a discussion about the propagation of the errors caused by the resolution of the devices.
Following are reported the resolution of the devices used to take the measurements:

- PT100: ± 0,01 °C
- Interrogator: ± 0,0008 nm
- Caliber: ± 0,05 mm
- $K_{corrective\ strain}$: ± 0,0011
- Micrometer: ± 0,01 mm

Considering the reported resolution, are analysed two different situations starting from the data obtained with the thermal tests: the minimum and maximum possible values of K_T with the data ranging in the resolution constraints.
The result is the following uncertainty about the K_T value:

$$R_{K_T} = \pm 0{,}00002\ nm/°C$$

This uncertainty combined with the resolution of the interrogator produces an uncertainty about the temperature of:

$$R_{°C} = \pm 0{,}025°C$$

For the resolution of the results about the thermal compensation, it is taken into account the value of the error about the corrective coefficient $K_{corrective}$ found by Candiano [8]; the result is an uncertainty of:

$$R_{\varepsilon} = \pm 0{,}0006\ \mu\varepsilon$$

4.2 Thermal analysis results

In this section are presented the results obtained during the tests for the thermal characterisation of the FBGs, the goal of these tests is to find a configuration which allows obtaining results without huge errors and without huge external disturbances. The selected configuration will be used then to conduct the tests about the thermal compensation.

4.2.1 First layout results

As shown in Figure 4.1 the first results obtained aren't linear and are affected by a huge hysteresis cycle, this is caused by an incorrect placement of the FBG that is in contact with the metal. The FBG and the PT100 are sensing different changes in temperature and the try to link one to the other leads to this error: the PT100 is sensing a temperature that is similar to the one of the Peltier cell, not perfectly the same as it is reported below; the FBG of the optical fiber is measuring a temperature that is a middle between the hot Peltier and the aluminium that is at a lower temperature because of his thermal capacity.

The not linear response is caused by the different time used to take the measures: a longer time lets the aluminium to warm up and the wavelength rises; when the temperature is lowered again the metal block is still heating up producing the visible increase in wavelength even if the PT100 is showing a decreasing of the Peltier temperature.

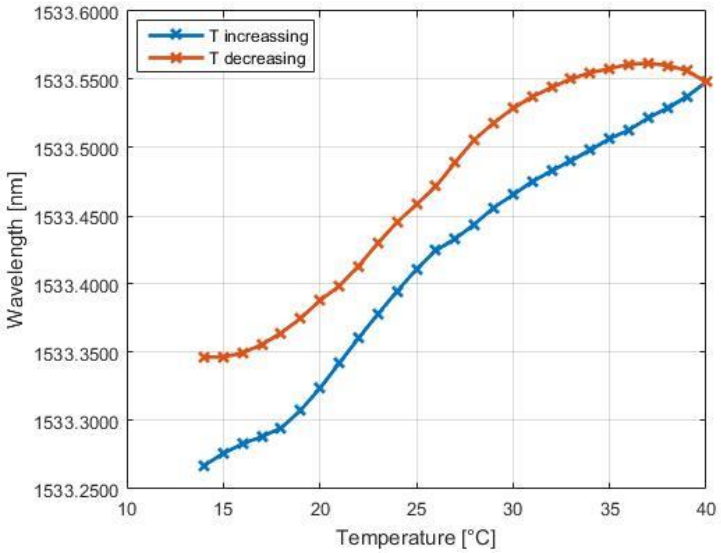

Figure 4.1: hysteresis caused by thermal capacity

After the repositioning of the fiber perfectly between the Peltier and the PT100, the results are linear but quite different from the theoretical ones, you can compare the equation of the linear fit in Figure 4.2 and the mean of the results in
Table 4.1 with the theoretical equation in chapter 2.2.1.
The main problem of this configuration is the huge variation in the results simply changing the way the fiber is positioned and the time left at the temperature to stabilize; in Figure 4.3 the wavelength is taken after 30 seconds from the reaching of the desired temperature, in Figure 4.2 the wavelength is taken after 2 minutes, the difference in the linear coefficients of the equations is about 44%; again it can be referred to
Table 4.1 for the value of the standard deviation, is also possible to see that the maximum value of K_T is twice the minimum one.

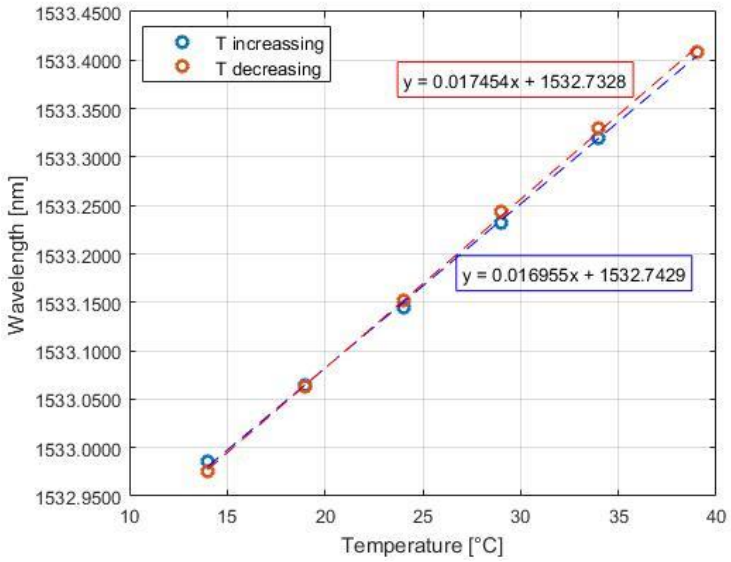

Figure 4.2: linear response, 2 minutes to stabilize temperature

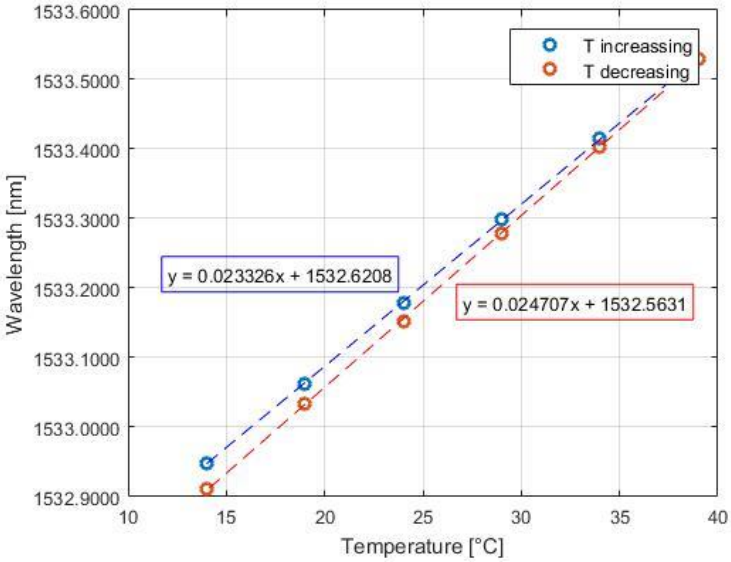

Figure 4.3: linear response, 30 seconds to stabilize temperature

The main source of these errors is the uncertainty about the actual temperature that the PT100 is sensing, with these tests it was understood that the PT100 is poorly isolated and is affected by the temperature of the cold metal surrounding it, so the PT100 temperature is lower than the one of the Peltier and the FBG leading to incorrect results. This problem is identified analysing the behaviour of the PT100 and the Peltier cell; this behaviour is

shown in Figure 4.4 and Figure 4.5. In Figure 4.5 is visible the current supplied to the Peltier cell, compared with the Figure 4.4 were is shown the temperature measured by the PT100 it is clearly visible a huge discrepancy: even if the PT100 is not sensing changes in temperature the current is decreasing, this is caused by the aluminium that is heating up and the Peltier needs a lower temperature and less power to maintain on the PT100 the desired temperature; the FBG is sensing a temperature value between the one of the PT100 and the one of the Peltier, so the wavelength is changing although it seems that the entire system is in a steady state condition.

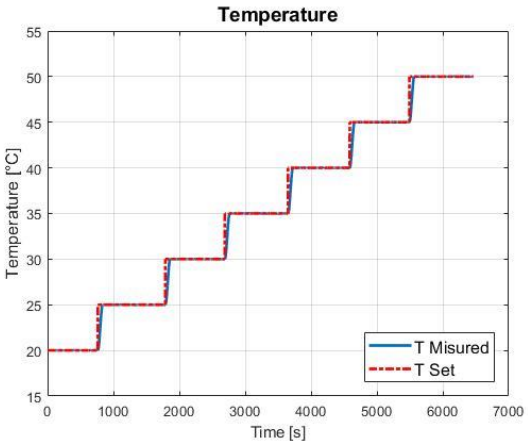

Figure 4.4: temperature measured by the PT100

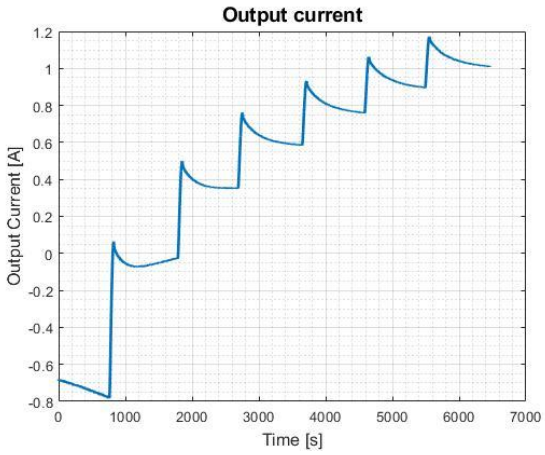

Figure 4.5: current supplied to the Peltier

Another problem encountered is the difficulty to place the FBG perfectly under the PT100 and in the same time be sure that the Peltier is in contact with the metal on both sides, also a little layer of air between the Peltier and the metal can lead to an increase in the power requested and in the consequent shut off of the power supplier.

Besides the uncertainty of the temperature measured and so the linear coefficient with a too high value respect of the theoretical one, there is another huge issue: the impossibility to replicate a certain test obtaining a result similar to the others obtained in the same way. Table 4.2 contains the results obtained for different tests; the first column indicates the time between two following steps, while the others the results obtained using the time indicated; first of all is visible the difference between the mean value of K_T take using different resting time, but the biggest issue is visible comparing the minimum and

maximum values of the linear coefficient, the error between these two values are reported in the column "Error" in percentage; even if it is maintained a defined step time the error between two set of measures could be about the 91% and this is unacceptable.

Table 4.1: results considering the entire set of measurement

	Values	Unit of measure
Bragg wavelength	1533,09	nm
Mean value of K_T	0,01969	nm / °C
Minimum value of K_T	0,01542	nm / °C
Maximum value of K_T	0,03008	nm / °C
Standard deviation	0,00367	nm / °C

Table 4.2: results subdivided by time the fiber has been kept in temperature, the results are in [nm/°C]

Time	Mean value	Maximum value	Minimum value	Error
5 minutes	0,01592	0,01642	0,01542	6 %
2 minutes	0,01872	0,02157	0,01605	34 %
1 minute	0,02404	0,03220	0,01685	91 %
30 seconds	0,02066	0,02471	0,01718	44 %

4.2.2 Second layout results

In this section are reported the results obtained with the series of tests made using the second layout; the first visible characteristic is the linear response; in Figure 4.6 are reported for reference the values of a test made with this layout where it could be seen the linearity of the response, but also the high value of the coefficient.

In Table 4.3 are shown the mean value of the linear coefficient and the standard deviation, the deviation is lower compared to the one of the previous series of tests and also the difference between the maximum and minimum value is significantly reduced, but the mean value is again too high.

The cause has been identified in the air layer surrounding the PT100, at first it was thought that the air would create an insulating layer, but actually, it induces a thermal flow resulting in an increase of the temperature of the Peltier and so an increase of the wavelength shift.

Unlike in the layout of the previous section, the values of K_T are closer to the average value because of the reduced thermal capacity, the origin of the error is moved from the thermal inertia to the thermal flow that is independent from the time the fiber has been kept in temperature.

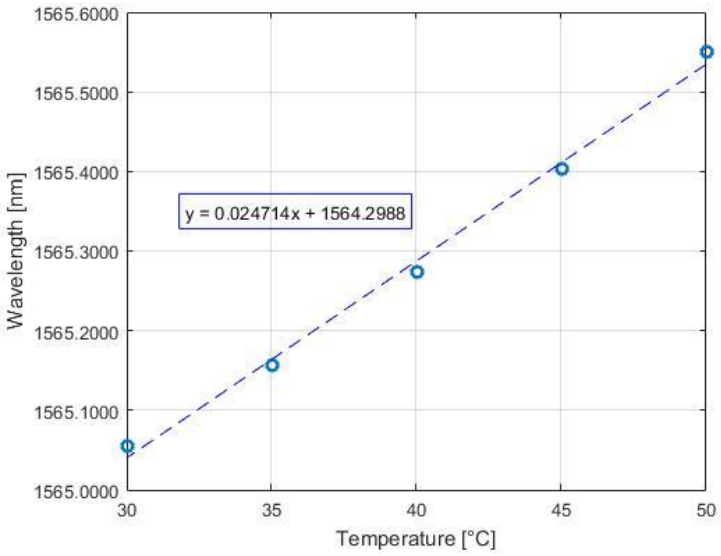

Figure 4.6: second configuration test

Table 4.3: Results

	Values	**Unit of measure**
Bragg wavelength	1565,07	nm
Mean value of K_T	0,02622	nm / °C
Minimum value of K_T	0,02471	nm / °C
Maximum value of K_T	0,02793	nm / °C
Standard deviation	0,00131	nm / °C

4.2.3 Third layout results

The third layout with the water system, as shown later, is the configuration that permits to obtain the results with lowest errors respect of the theoretical equations.
The data obtained with this configuration shows a good linearity like the other with the previous layout, the main difference is the value of the K_T that now is in the range identified in section 2.2.1. The results show that the Peltier cell is able to warm the water and this one creates a homogeneous temperature area, so now it is sure that the temperature measured by the PT100 is the same measured by the FBG.
In Figure 4.9 is presented the data obtained with the .log file and processed in Matlab, in particular, is shown the wavelength in function of the temperature measured by the PT100, is easily visible the linearity of the results, it can be taken as a comparison the red line that represents the linear best fit; in this test is imposed to the Peltier cell to maintain a constant temperature increasing rate.
To take the data it is also used the temperature step system, as visible in Figure 4.10 and Figure 4.11 the current intensity on the Peltier has the same trend of the temperature except for the initial transient, this transient is caused by the PID controller that is supplying to the Peltier cell a huge power to warm rapidly the water mass.
In Figure 4.11 is presented a comparison between the current supplied to the Peltier cell with this new water system and the current supplied with the old system with the aluminium blocks; is visible that the system is slower, the different response is due to the water mass to be warmed. In the figure is also visible that, spent the initial transient, the current supplied is steady; actually it decreases a little, this is due to the slight temperature rise that reduces the error and so the current supplied.

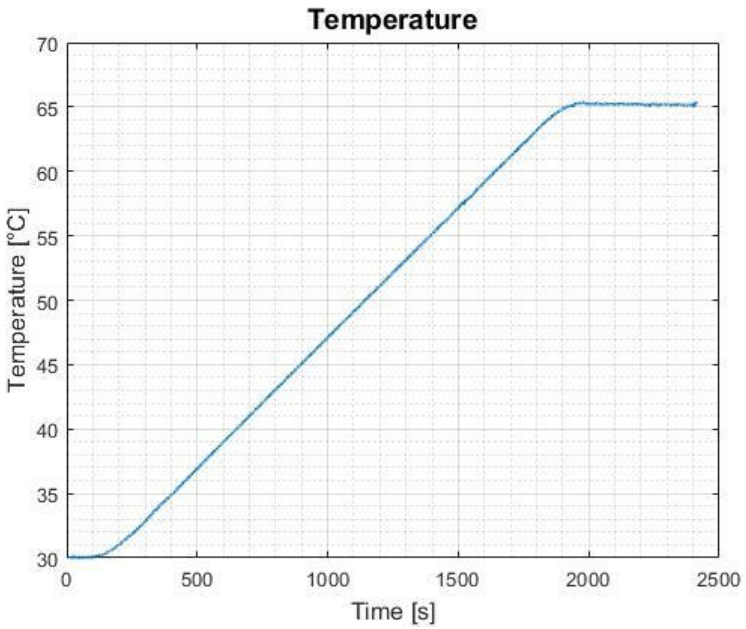

Figure 4.7: temperature measured by the PT100

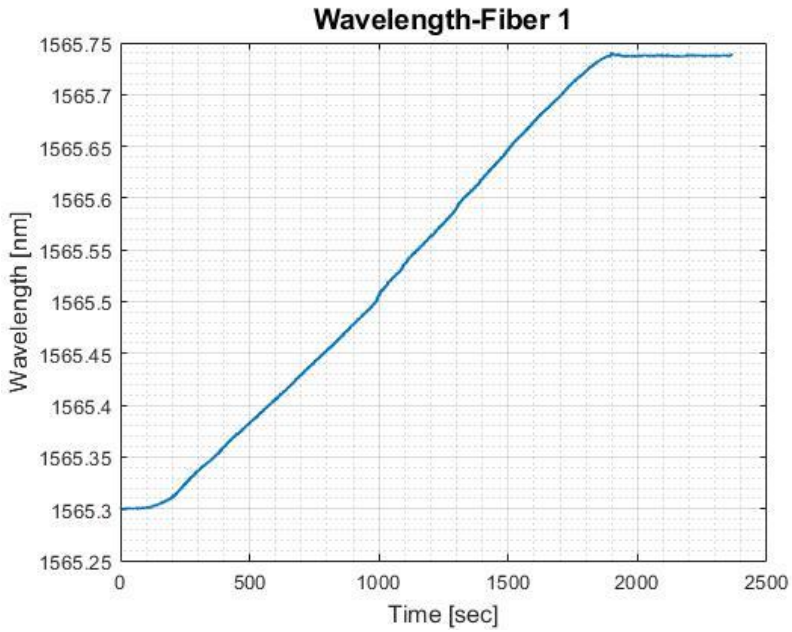

Figure 4.8: wavelength reflected by the FBG

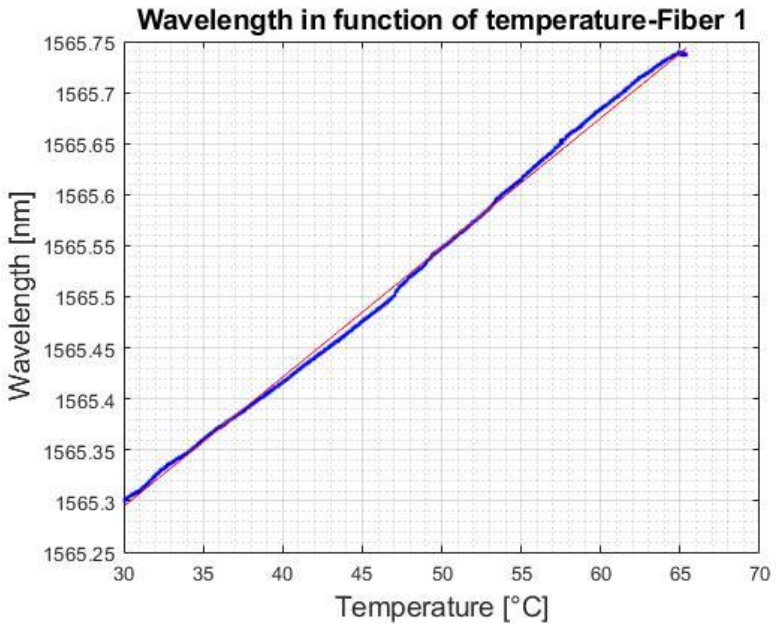

Figure 4.9: wavelength reflected by the FBG in function of the temperature measured by the PT100

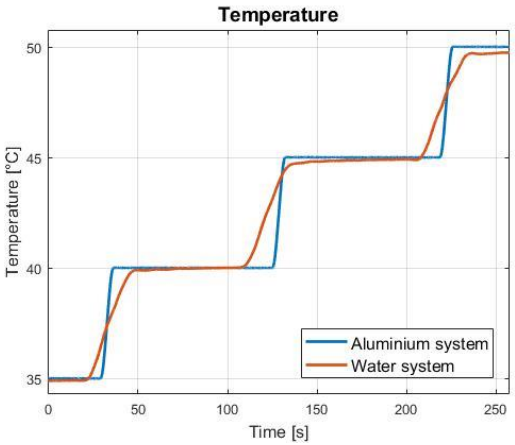

Figure 4.10: temperature sensed by the PT100

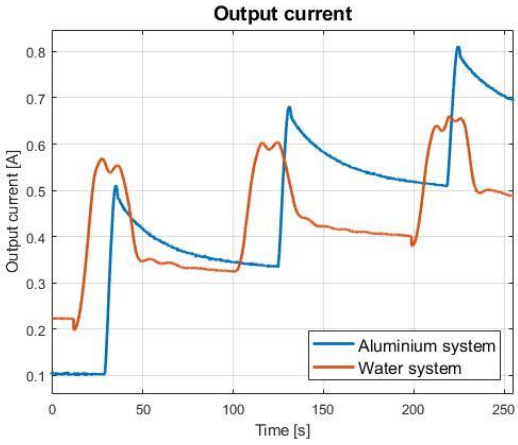

Figure 4.11: current supplied to the Peltier cell with the new layout comparing to the old one

The data for this configuration are taken with two different methods: writing down the wavelength and temperature values when this one is stable, or via the .log files that are post processed with a Matlab script; the results are reported in Table 4.4 and Table 4.5.
It is possible to see first of all the low value of the standard deviation and the low error between the maximum and the minimum value of K_T, the low dispersion of the data

permits to replicate the tests; a replicable test is an important point in the identification of the correct layout.

There is a small difference between the value of K_T found via the manual mode respect of the one found via the log file, the difference is about 1,4 %; this is due to the different way the data are taken: writing takes place when the values are as stable as possible and the transient is ended; instead the log file takes the data all the time taking into consideration also the transient, between the PT100 and the FBG there is a little difference in the response speed and the result is shown in Figure 4.12.

Table 4.4: results obtained writing down the wavelength and the temperature

	Values	**Unit of measure**
Bragg wavelength	1565,07	nm
Mean value of K_T	0,01208	nm / °C
Minimum value of K_T	0,01177	nm / °C
Maximum value of K_T	0,01237	nm / °C
Standard deviation	0,00020	nm / °C

Table 4.5: results obtained with the log files

	Values	**Unit of measure**
Bragg wavelength	1565,07	nm
Mean value of K_T	0,01225	nm / °C
Minimum value of K_T	0,01166	nm / °C
Maximum value of K_T	0,01268	nm / °C
Standard deviation	0,00025	nm / °C

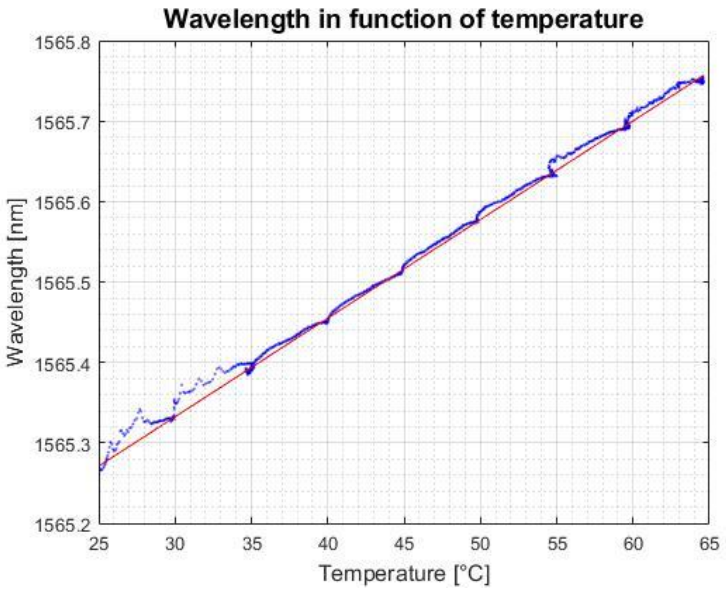

Figure 4.12: discrepancies between wavelength and temperature

4.2.4 Fourth layout results

Identified in the configuration presented in chapter 3.6 the best design to be used for the different thermal tests of the fiber, the configuration is changed to permit the tensioning of a fiber while its FBG is immersed in the water; the result is the design of chapter 3.7.
This layout is used to perform thermal tests to see how the fiber reacts at temperature changes with different levels of strain, these tests are conducted before the thermal compensation in order to be sure about the behaviour that will have the fiber when it will be tensioned in the future tests.
For this kind of tests is used the fiber that will be used for the strain measurements, thanks to the micrometre it is possible to tension the fiber and then conduct the thermal tests.
The results are reported in the following images, the Figure 4.13, Figure 4.14 and Figure 4.15 refers to the test number 54 where the locked fiber is loose; it is possible to see that the wavelength of the locked fiber, the wavelength of the not locked fiber and the temperature have the same trend, especially when the temperature is stable also the wavelength of both fibers does not change.

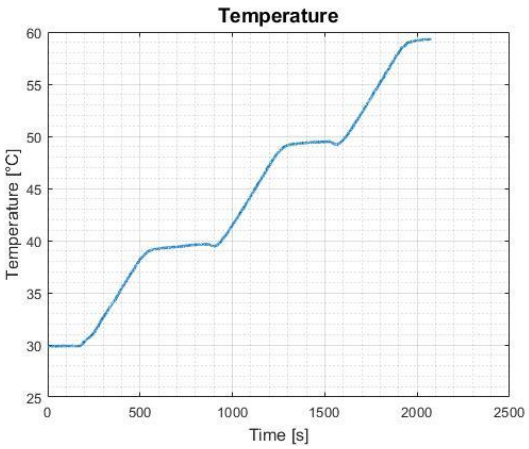

Figure 4.13: no prestressing, temperature

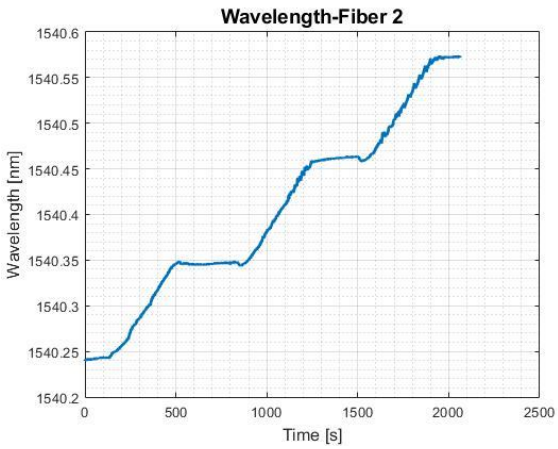

Figure 4.14: no prestressing, locked fiber wavelength

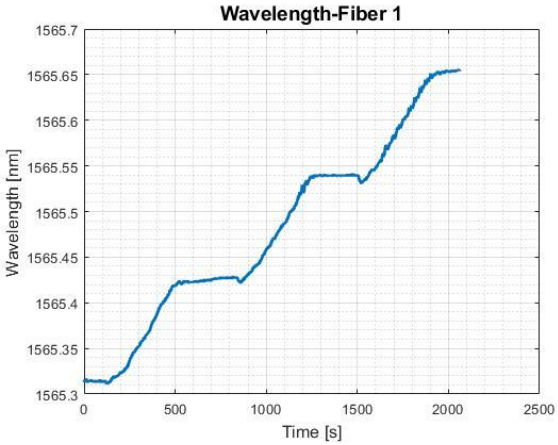

Figure 4.15: no prestressing, not locked fiber wavelength

In Figure 4.16, Figure 4.17 and Figure 4.18 the locked fiber is deformed to about 434 με, it is visible a first discrepancy: even if the temperature is stable the wavelength of the locked fiber is still changing; however this trend is not visible in Figure 4.18 where is shown the wavelength of the free fiber.

In Figure 4.19, Figure 4.20 and Figure 4.21 the strain on the locked fiber is increased even more to about 5869 με and the effect highlighted before is still increased, again it can be compared Figure 4.20 with Figure 4.19, when the temperature is stable the wavelength of

the locked fiber is increasing, the last step is 10 minutes long and the wavelength has increased by 0,078 nm.

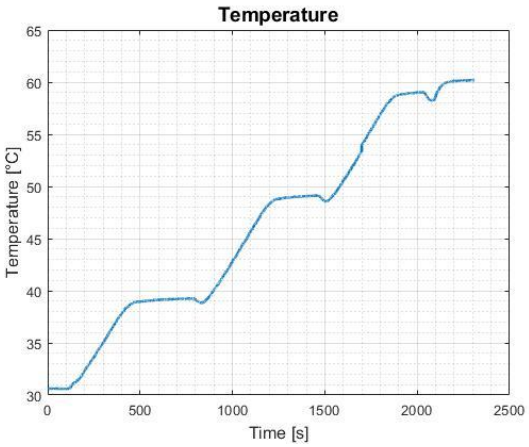

Figure 4.16: prestressing to 434 με, temperature

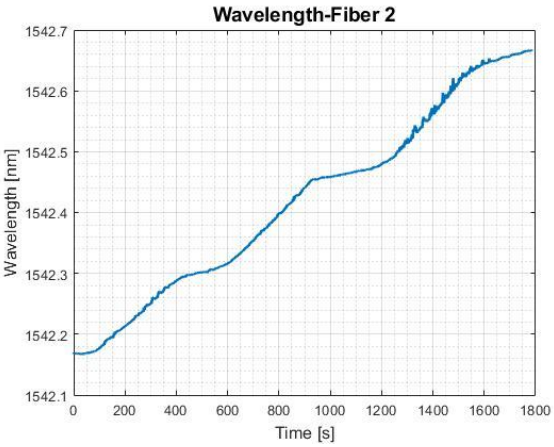

Figure 4.17: prestressing to 434 με, locked fiber wavelength

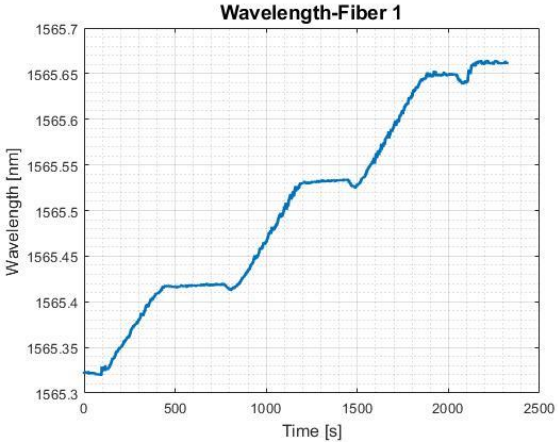

Figure 4.18: prestressing to 434 με, not locked fiber wavelength

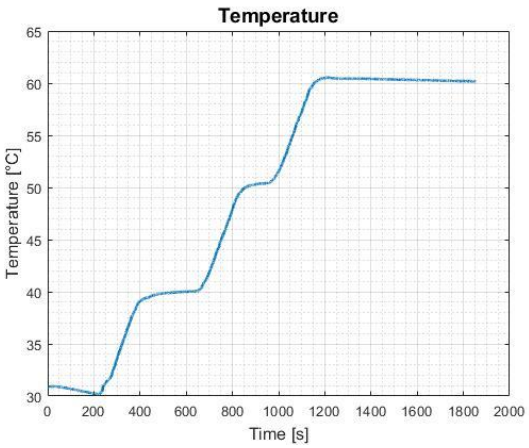

Figure 4.19: prestressing to 5869 με, temperature

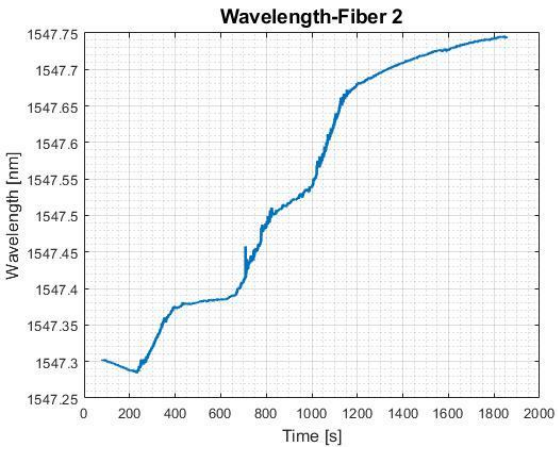

Figure 4.20: prestressing to 5869 με, locked fiber wavelength

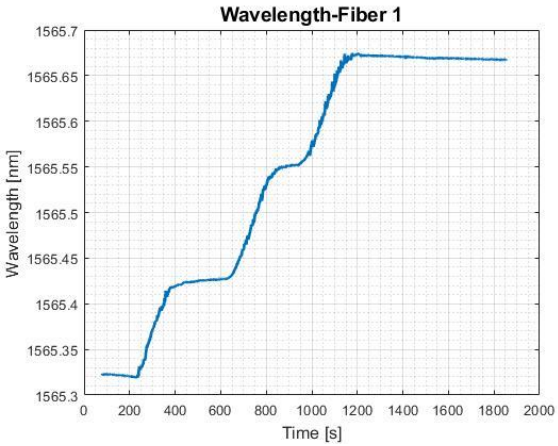

Figure 4.21: prestressing to 5869 με, not locked fiber wavelength

The first hypothesis about this behaviour is that the FBG was damaged because over-stressed, so it has been proceeded to change the locked fiber with a new one, but the results are the same as before as visible in Figure 4.22 and Figure 4.23 were the fiber is pretensioned to 526 με.

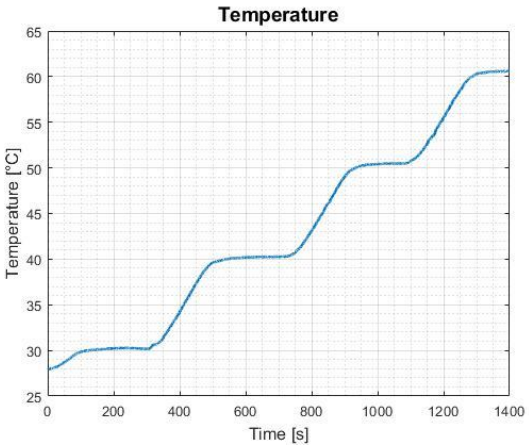

Figure 4.22: new fiber, prestressing to 526 με, temperature

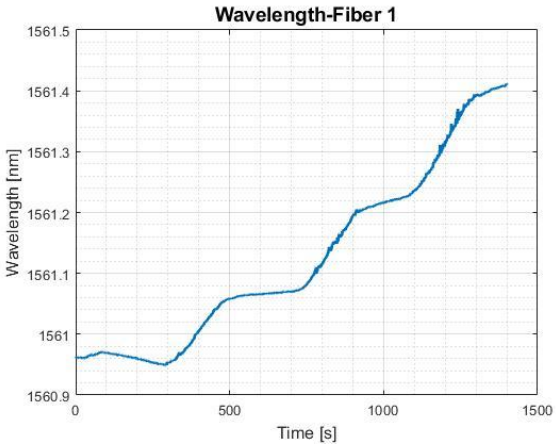

Figure 4.23: new fiber, prestressing to 526 με, locked fiber wavelength

This behaviour of the FBG leads also to an impossibility to calculate the right value of K_T and to an apparent increase of this one when the fiber is tensioned, the values of the coefficient are reported in Table 4.6 for the two fibers used and the different tensioning condition.

Table 4.6: values of K_T with different fibers and tensioning conditions

Bragg wavelength [nm]	**K_T for loose fiber [nm/°C]**	**K_T for tensioned fiber [nm/°C]**
1540,23	0,01123	0,01593
1560,09	0,01090	0,01498

Rejected the hypothesis of the damaged fiber another possibility could be the thermal expansion of the PLA which constitutes the water housing; the PLA has a thermal expansion coefficient of about $80x10^{-6}$ [1/°C], compared to the coefficient of the silica that is $0,5x10^{-6}$ [1/°C] it can be seen that there are two orders of magnitude between these two values, so the hypothesis of the thermal expansion could be possible.

To validate this hypothesis the design of the test bench is changed as described in chapter 3.7 to uncouple the water housing to the base for the fiber locking system.

In Figure 4.24 and Figure 4.25 are presented the wavelength of the locked fiber and the temperature steps with the fiber loose, comparing these two first figures with Figure 4.26

and Figure 4.27 where the fiber is tensioned to 1327 με it can be seen that there is no more the strange response of the wavelength when the temperature is stable visible in Figure 4.20; the response of the FBG is not changing with the pretensioning.

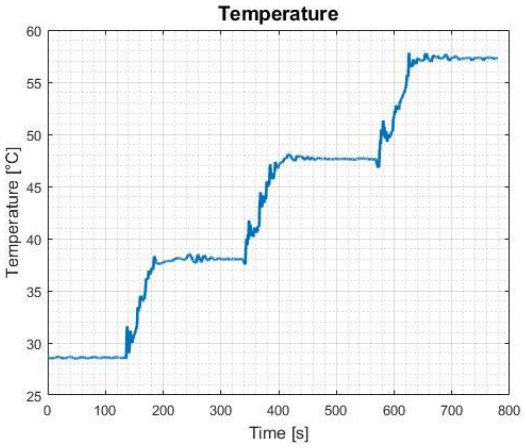

Figure 4.24: new layout, no prestressing, temperature

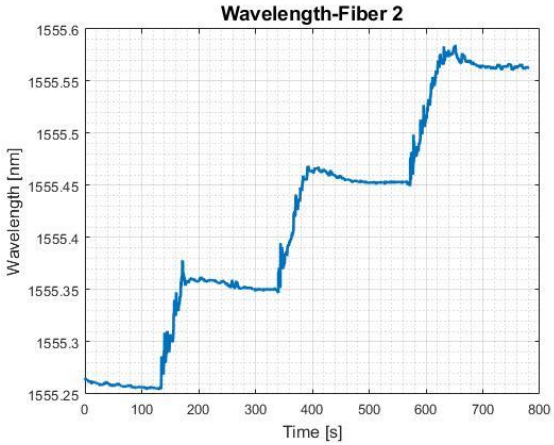

Figure 4.25: new layout, no prestressing, locked fiber wavelength

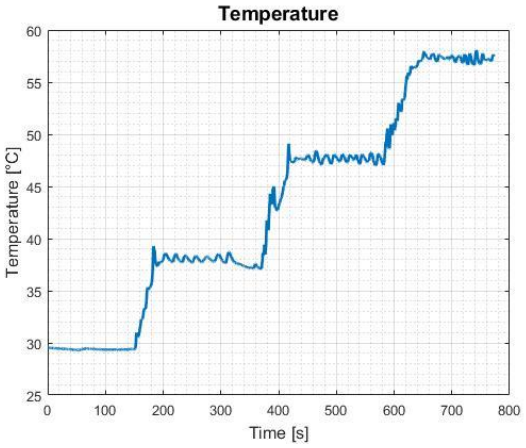

Figure 4.26: new layout, prestressing to 1327με, temperature

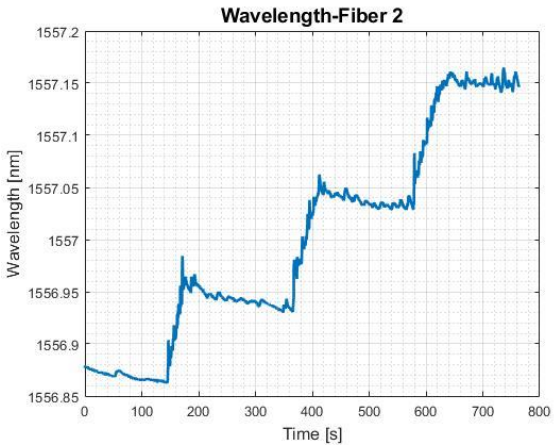

Figure 4.27: new layout, prestressing to 1327με, locked fiber wavelength

The oscillation of the temperature, and consequently the one of the wavelength, are caused by an instability of the Peltier microcontroller unable to maintain a stable

temperature value; the slight reduction in wavelength is caused by the deterioration of the glue explained in chapter 4.3.3.

In the Table 4.7 and Table 4.8 are reported the results obtained for the two fiber used in anticipation of the thermal compensation tests, a fiber is used for the strain measurements and the other for the temperature measurements.

The results are quite accurate and the standard deviation is really low, two orders of magnitude below the K_T value; also the difference between the maximum and minimum value is low, about 2,6 % for the fiber dedicated to the strain and 3,7 % for the fiber dedicated to the temperature.

Could be noticed a little difference between the values of K_T found with this layout respect of the one found with the design explained in chapter 3.6, the relative results are visible in Table 4.4; this error is about 4,4 % and could be neglected because supposing an increase in temperature of 100°C the resulting error in the induced wavelength shift is only 42 με. The source of this error can be detected in the thermal expansion that was affecting the results of the Table 4.4 via the sealant that was glued on the fiber and induced a little strain when the PLA was expanding.

Table 4.7: value of K_T for the fiber used to measure the strain

	Values	**Unit of measure**
Bragg wavelength	1560,09	nm
Mean value of K_T	0,01080	nm / °C
Minimum value of K_T	0,01069	nm / °C
Maximum value of K_T	0,01097	nm / °C
Standard deviation	0,00012	nm / °C

Table 4.8: value of KT for the fiber used to measure the temperature

	Values	**Unit of measure**
Bragg wavelength	1565,07	nm
Mean value of K_T	0,01157	nm / °C
Minimum value of K_T	0,01130	nm / °C
Maximum value of K_T	0,01173	nm / °C
Standard deviation	0,00019	nm / °C

4.2.5 Summary of the results obtained

The last configuration presented is used to test different fibers with different Bragg wavelength in order to collect data and understand the response of the FBG in not ideal conditions, the summary of the results obtained is reported in Table 4.9 and Table 4.10.
In Table 4.9 are shown the linear coefficients K_T related to each fibers, it is clearly visible the absence of a trend between the value of these coefficients and the Bragg wavelength, probably this is due to the little difference in the reflected wavelength and the not ideal condition of the test.
In Table 4.10 is reported the mean value of K_T relative to all the data collected, without distinguish the different kind of FBG; it is possible to see that this mean value is near the K_T found for the different fibers, the low dispersion of the data is also highlighted by the low value of the standard deviation which is two orders of magnitude below the linear coefficient K_T.

Table 4.9: result of thermal analysis using different fibers

Bragg wavelength [nm]	**Mean value of K_T [nm/°C]**	**ΔT using 0,01110 nm/°C [°C]**
1540,18	0,01163	4,7
1560,09	0,01080	-2,7
1565,07	0,01157	4,2

To point out the low difference in the results obtained using the mean K_T of Table 4.10 instead of the one relative to each FBG, in Table 4.9, third column, are reported the error in temperature considering K_T = 0,01110 nm instead the one of that particular FBG and an increase of temperature of 100°C respect of the calibration point; it is possible to see that the error is always below 5°C.
The conclusion is that is possible to use a mean K_T for all the fiber used if an accuracy of 5% is enough; for particular applications where is needed a better accuracy is recommended to calibrate each FBG separately.

Table 4.10: mean value and standard deviation using whole data

Mean value [nm/°C]	Standard deviation [nm/°C]
0,01110	0,00061

4.3 Thermal compensation results

The thermal compensation consists in taking information from two different FBG and use the data about the temperature to compensate the data coming from the FBG used for the strain measurements.

Compensation is required because, as visible in equation (2.10) of chapter 2.2.1, the wavelength shift is caused by a mechanical deformation, a thermal deformation and the change in the refractive index induced by the change in temperature; to have accurate results about the strain it is necessary to subtract the contribution of the temperature to the wavelength shift.

The compensation for these tests is made thanks to a Matlab script in which the wavelength shift of the temperature FBG is used to calculate the temperature difference respect of the calibration point; this temperature difference induces a wavelength change that is subtracted to the wavelength shift of the strain FBG to obtain the correct value of the strain; this process is summarized in Figure 4.28.

Below are reported the Figure 4.29 and Figure 4.30 to show the importance of the thermal compensation in case of change in temperature; in Figure 4.29 is reported the wavelength measured with the interrogator, the data are only taken during the steady sections and are not plotted the transients; is visible the translation of the wavelength induced by the thermal shift as reported by equation (2.10) in chapter 2.2.1.

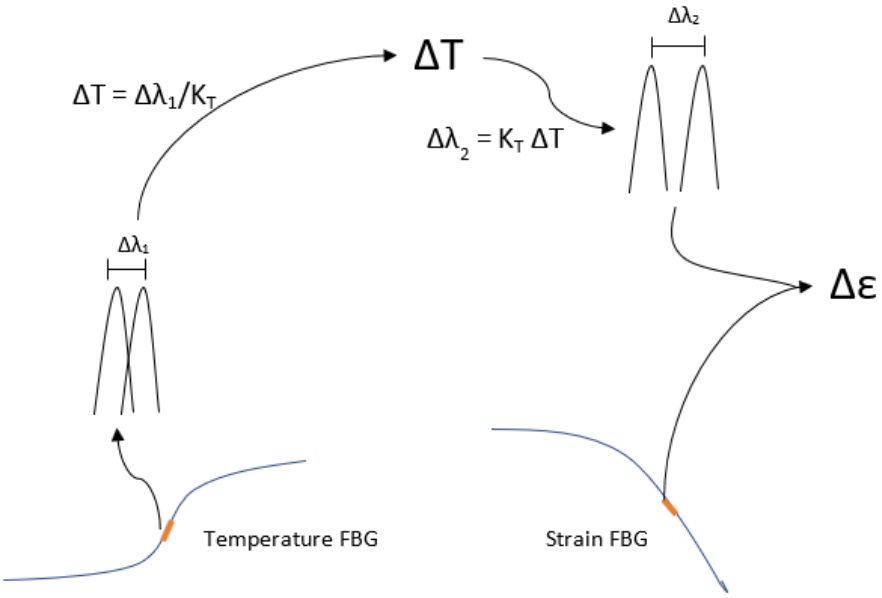

Figure 4.28: process implemented in the Matlab script

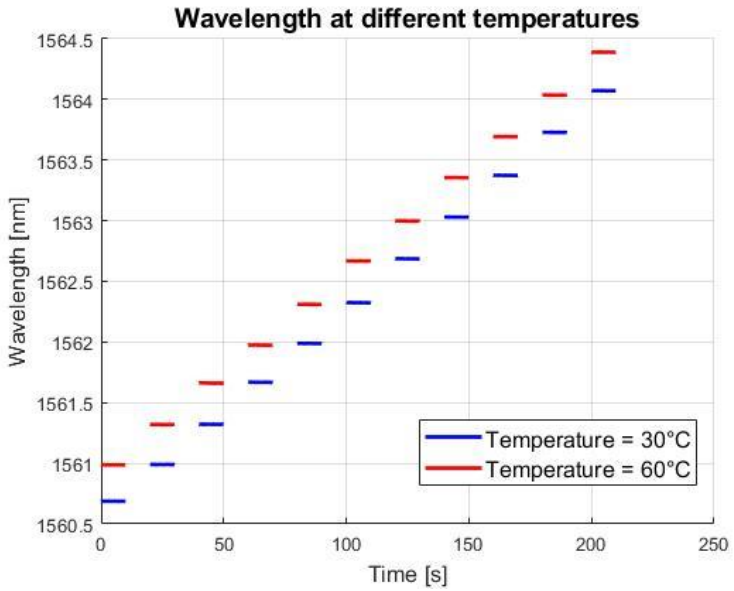

Figure 4.29: wavelength for strain tests at 30°C and 60°C

This wavelength shift leads to an error in the strain, and consequently in the displacement, if it is calculated with an equation that does not take into account the contribution of the temperature, like the one below implemented in the script used:

$$\Delta\lambda_B = \lambda_B(1 - p_E)\Delta\varepsilon \tag{4.1}$$

This error is clearly visible in Figure 4.30 where the prestressing point and the step are the same for the two tests, but it seems that there is a difference of 0,05 mm between the two sets of measurements, with a length of the fiber of 172,75 mm the error is 289 με; this is obtained with a temperature difference respect of the calibration point of only 30°C, being linear the temperature equation take into account it can be easily understood that, if the temperature difference is about 100°C, the error increase to 0,17 mm and 1000 με and is not negligible.

In Figure 4.31 is visible the wavelength of the strain tests made at 60°C compensated taking into account the contribution of the temperature shift, now the difference between these values and the one taken at the calibration temperature are quite the same except for little errors due to the resolution of the micrometre manually operated.

In the compensated tests the error between the wavelength measured at the calibration temperature and the wavelength measured at 60°C and then compensated is only 4 με, considering a fiber length of 172,75 mm the error is 0,0007 mm; this value is two orders of magnitude below the resolution of the micrometre; also with a temperature shift of 100°C the error is about 0,0023 mm; it is recalled that the resolution of the micrometre is ± 0,01 mm.

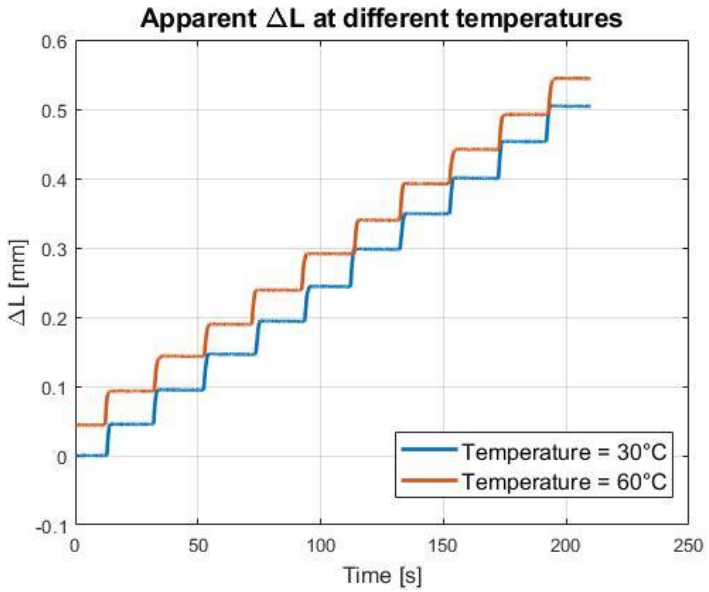

Figure 4.30: apparent deformation applied for the strain tests at 30°C and 60°C

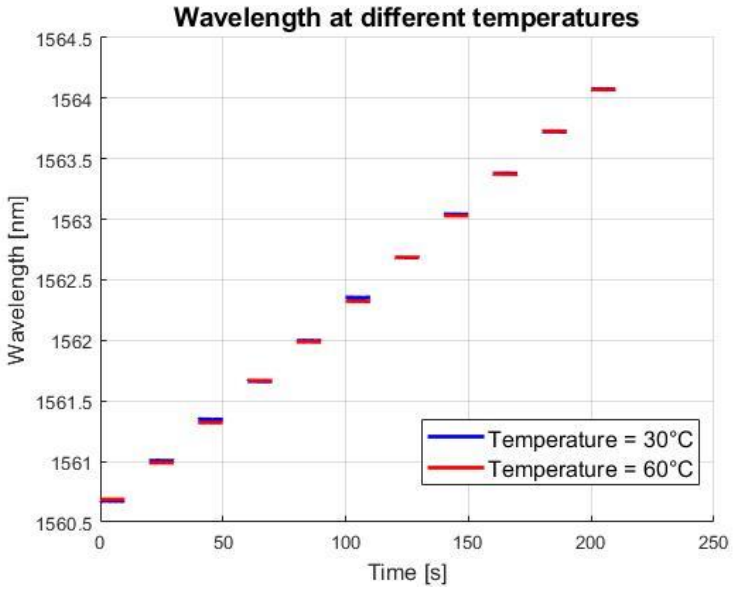

Figure 4.31: wavelength of strain tests at 30°C and 60°C compensated

4.3.1 Strain results analysis

A first needed analysis is the one about the pure strain response of the FBG to be sure that the results obtained are not affected by errors. All the data collected for the thermal compensation tests are processed in a first time thanks to the Matlab script developed in the previous thesis; this script is used only for the pure strain and does not consider the thermal contribution.

The data are acquired via a series of steps of precise dimension, then the script compares the obtained strain with the theoretical one calculated knowing the length of the fiber between the two locking system, called L_0, and applies a corrective coefficient to take into account all the deformations of fiber coating, micrometre system and locking epoxy resin; the comparison between the coefficients found by Giancarlo Candiano and presented in his thesis and the coefficients found with the thermal compensation tests is used to validate this particular configuration.

In Table 4.11 are reported the validated values of the corrective coefficient in function of L_0 [8]; in Table 4.12 are presented the strain corrective coefficients obtained in the thermal analysis tests; it is possible to see that the values obtained for the two different lengths of the fiber are a little different. The longer one is referred to a fiber glued with the old epoxy glue and is affected by the visco-elastic deformation highlighted in chapter 4.3.3; the shortest L_0 refers to a new fiber locked with the new glue, in this case, the value of the corrective coefficient is in the range identified and validated by Candiano in his thesis; the same data are plotted in Figure 4.32.

It must be underlined that another source of errors is the difficulty to precisely measure the actual length of the fiber between the two locking system due to the presence of the PLA block; it was necessary to subdivide the fiber into two segments and sum up the two measurements, this process introduces some errors.

Table 4.11: strain corrective coefficient for different fiber length as described in the thesis of Giancarlo Candiano

Fiber length [mm]	Corrective coefficient [-]
53,59	1,1248
151,16	1,0212
228,94	1,0012

Table 4.12: strain corrective coefficient obtained in the thermal analysis tests

Fiber length [mm]	Corrective coefficient [-]
161.15	1,0219
172.75	1,0349

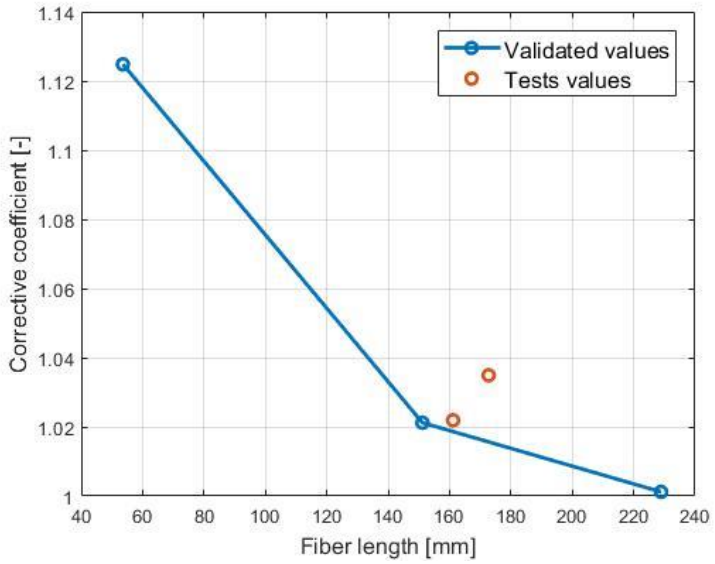

Figure 4.32: comparison between the validated values of the strain corrective coefficient and the one found during the thermal compensation tests

4.3.2 Thermal compensation results analysis

Verified the accuracy of the strain measurements made with this configuration, it can be put together the two effects relative to the mechanical deformation and thermal wave-length shift to do the thermal compensation.

The experiments are made using the following steps:

- The two fibers are brought to a desired starting temperature for the calibration and their respective Bragg wavelength are noted down; the fiber used to measure the strain must be prestressed.
- A strain test is made increasing the deformation with the micrometre.
- The micrometre is set again to the prestress position and the temperature is increased to another desired value.
- Another strain test is made.

The data obtained thanks to these series of tests are then analysed with a Matlab script to subtract to the wavelength shift of the strain fiber the contribution of the temperature; the free fiber is used to calculate the temperature change.
The thermal compensation data analysis is made in two ways: using the linear coefficient K_T specific for each fiber, or using an unique coefficient for both fibers; the values of these K_T and the way they are found is explained in chapter 4.2.5; the wavelength obtained thanks to the compensation is then compared with the wavelength obtained with the test at the calibration point and a resulting strain error is calculated.

Table 4.13: example of results of thermal compensation test with calibration point at 30°C

Temperature [°C]	**Mean error with specific K_T [με]**	**Mean error with common K_T [με]**
40	4,1069	9,6470
50	2,6689	15,1840
60	7,5941	26,0593

In Table 4.13 are reported as examples the results of a thermal compensation test to show the trend of the error; this error refers to the strain measured with the compensation respect the one measured at the calibration point.
The entire results obtained are summarised in Table 4.14; it is possible to see a difference of one order of magnitude in the error resulting from the using of a common K_T for all the fibers and from the using of a specific one.
To better understand the entity of the errors, the same results are reported in millimetres in Table 4.15 considering a length of 172 mm between the two locking system; even in

the worst case, the error is 0,0062 mm, one order of magnitude below the resolution of the micrometre that is 0,01 mm.

The conclusion is that an individual calibration of each FBG is not necessary: in fact, the use of a common value is able to ensure an accuracy higher than the resolution of the tensioning system (in other words, in this case, the micrometre is the system element that limits the accuracy of the aforesaid measurements).

Table 4.14: summary of the strain errors obtained after the thermal compensation

	Mean error [με]	**Max error [με]**	**Min error [με]**
Specific K_T	6,1446	15,5351	0,4099
Common K_T	21,0610	35,9759	5,3292

Table 4.15: summary of the error in mm considering a length of 172 mm

	Mean error [mm]	**Max error [mm]**	**Min error [mm]**
Specific K_T	0,0011	0,0027	0,0001
Common K_T	0,0036	0,0062	0,0009

It must be highlighted that the use of a common K_T for all the fiber, in the thermal compensation, is the same as not considering at all the K_T; this because from the wavelength shift of the temperature FBG is obtained the temperature change thanks to this K_T, then with the same K_T is obtained the wavelength shift of the strain FBG; it is easy to understand that this wavelength shift is the same.

The consequence is that, if it is required only a thermal compensation and not a direct measuring of the temperature, is not required the thermal calibration of the FBG; so is eliminated a step to put in place the sensor and the operation to compensate the strain is a simple subtraction of the temperature FBG wavelength shift.

4.3.3 Epoxy glue bonding problems

During the thermal compensation tests a problem relative to the locking system occurred; it is noticed a change in wavelength due probably to a slip of the fiber; this problem is clearly visible in Figure 4.33 where the micrometre is not moved after the tensioning step;

even if the micrometre is steady the wavelength is decreasing; also the results about the corrective coefficient obtained in chapter 4.3.1 shows a problem about the glueing system.

To identify the source of this behaviour some tests are performed, the possible causes could be:

- Failure of the bonding system after a period of time.
- PLA substrate not suitable for a good bonding over time.
- Wrong bonding procedure.
- Layer of glue too thin.
- Epoxy glue too old.

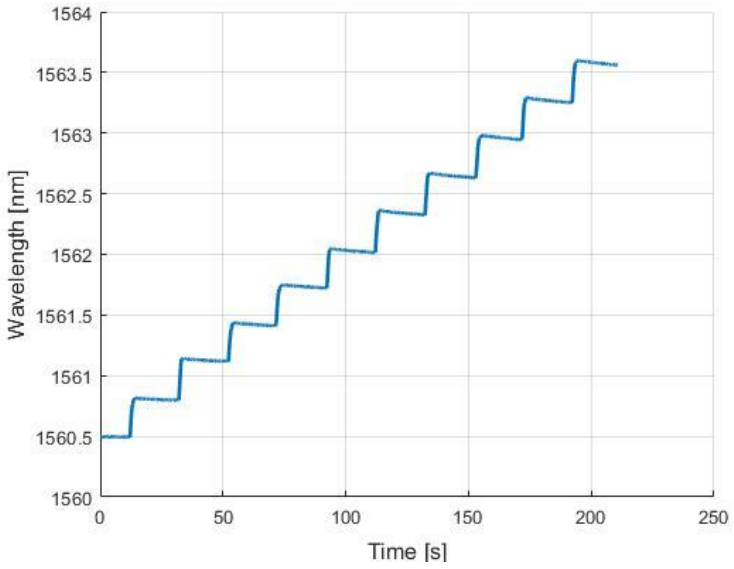

Figure 4.33: strain test with decrease in wavelength while deformation is constant

The presence of some strain measuring system used for the previous thesis still mounted permits to verify if the problem is caused by the first point; the substrate for the glue is PLA for one system and aluminium for another, this permits to verify the second point.

In Figure 4.35 and Figure 4.36 are shown the responses of the FBG mounted in June on a PLA substrate and on an aluminium substrate respectively; comparing the results with

the one visible in Figure 4.34, where are reported the data coming from the thermal compensation layout, it is clearly visible the absence of the wavelength decreasing while the fiber is stressed, decrease present in Figure 4.34; the conclusion is that the substrate and the age of the bonding are not affecting the results.

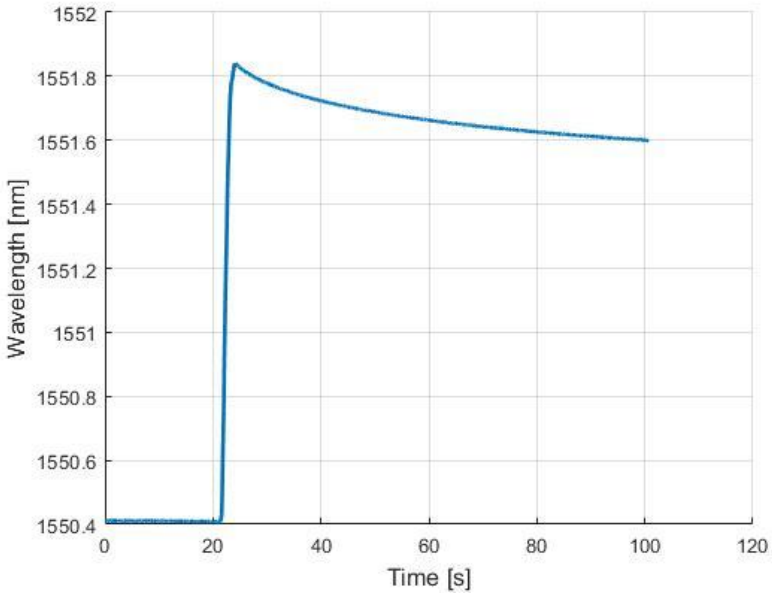

Figure 4.34: bonding made on the thermal compensation layout, PLA substrate

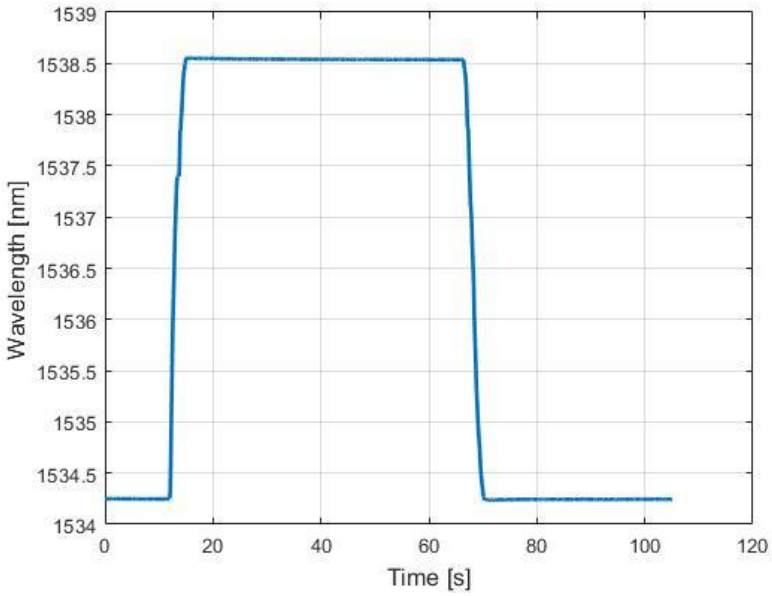

Figure 4.35: bond made in June, PLA substrate

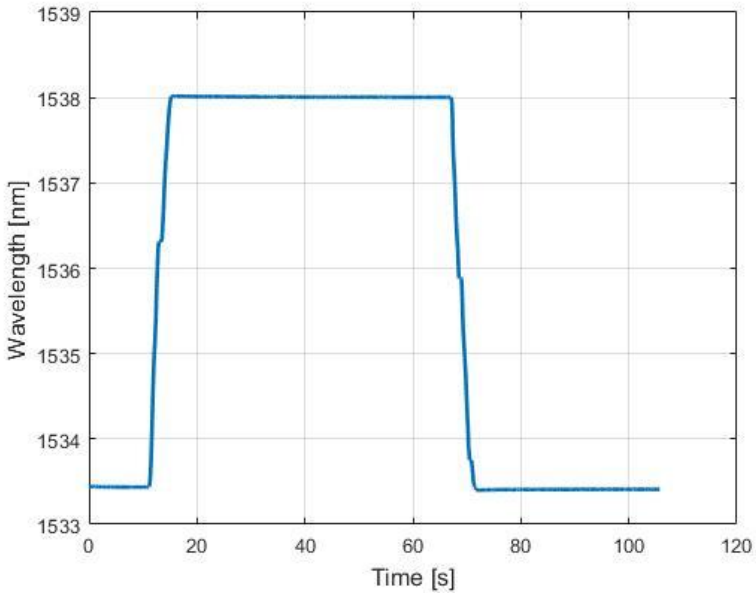

Figure 4.36: bond made in June, aluminium substrate

To check if the source of the problem is the third or the fourth point another fiber is glued with a thicker epoxy layer and paying attention to degrease the surface where the glue is applied.

The result of the test is reported in Figure 4.37 where is still visible the decrease of the wavelength; the conclusion is that the cause is not the bonding procedure or the glue layer thickness.

The last cause to be verified is the epoxy glue too old; so a new fiber is put in place using a new glue, the result is visible in Figure 4.39; to see better the behaviour of the two locking system the Figure 4.40 compares the wavelength obtained with the old epoxy glue and the wavelength obtained with the new one; the two Bragg wavelengths are different, so are reported only the relatives wavelength respect of the finish of the tensioning phase. The theory of the glue too old is also supported by the behaviour of the old epoxy bonding: when the strain is reduced the wavelength is increasing slightly as shown in Figure 4.38, this viscous-elastic behaviour is due to the glue outdated.

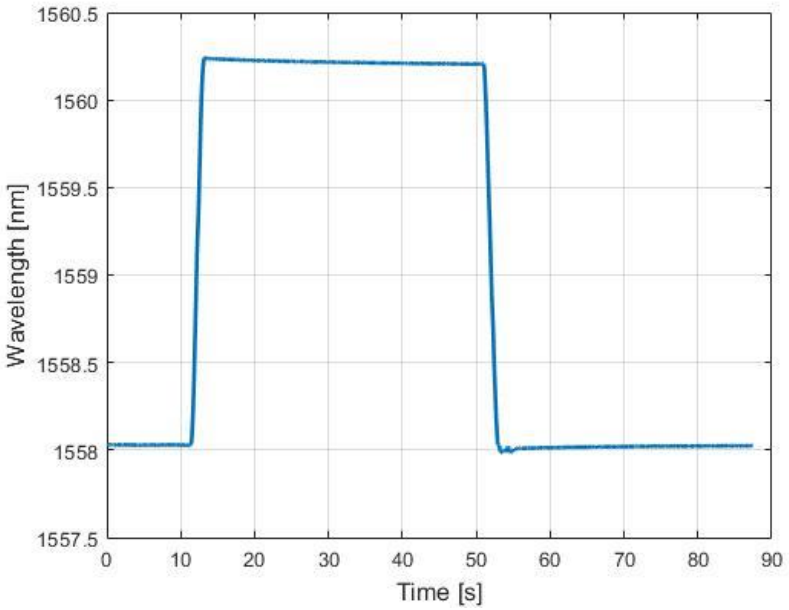

Figure 4.37: new fiber with thicker glue layer and degreased surface

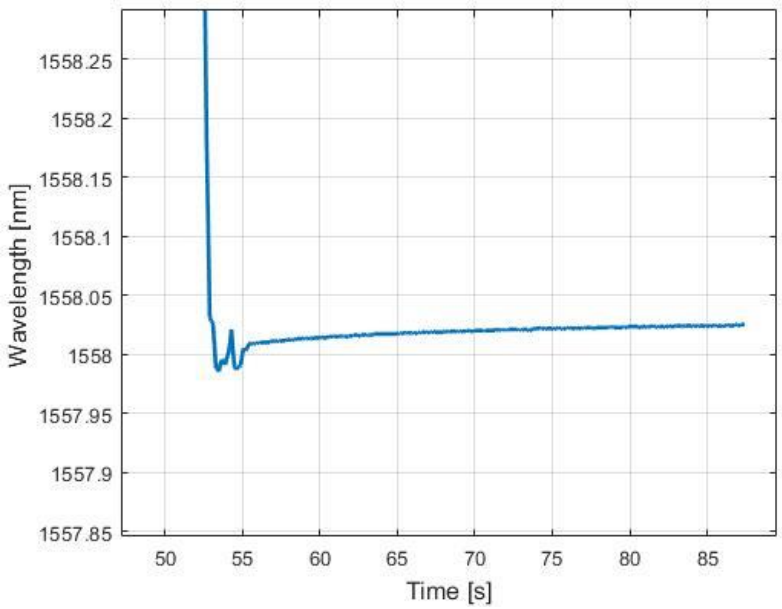

Figure 4.38: zoom of the last 30 seconds of Figure 4.37 to show the increasing of the wavelength when the strain is reduced

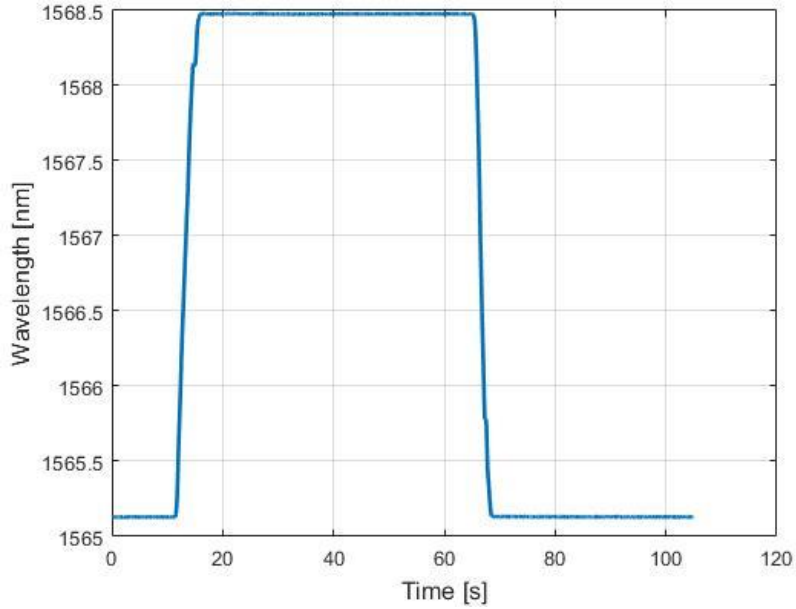

Figure 4.39: bonding made with new epoxy glue

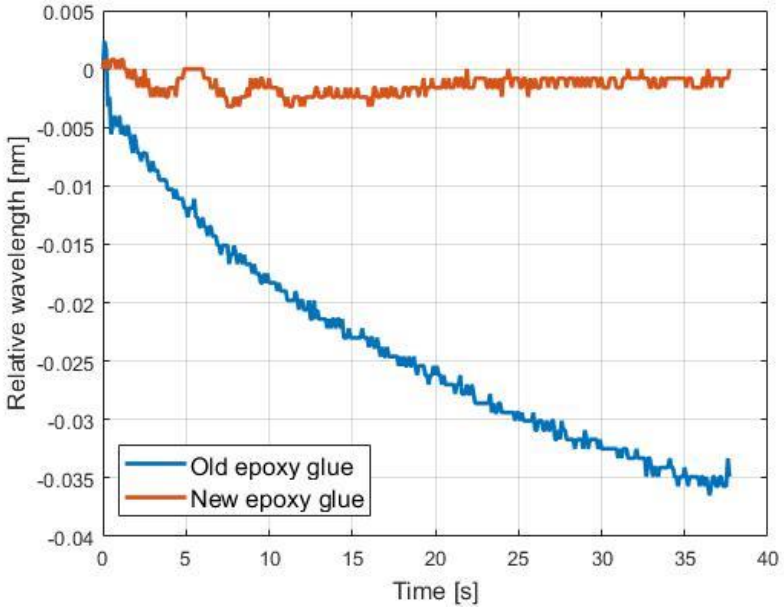

Figure 4.40: comparison between the response with the old glue and with the new one, wavelength are relatives

5 Conclusions and future developments

In this chapter are summarised the most important results obtained thanks to the different tests performed.

The main objectives of this thesis are: build a test bench useful to test the fiber reducing as much as possible the errors from external disturbances; derive from the data obtained with the different tests the behaviour respect of temperature change of the FBG in a not ideal condition; identify a proper way to perform the thermal compensation with a sufficient accuracy and in an easy way.

The design presented in chapter 3.7 is able to perform the tests on the thermal FBG obtaining results in the range reported by the theoretical equations in chapter 2.2.1; moreover it is possible with this layout to have the FBG of the fiber used for strain measurements in a controlled temperature area and with only one point with the sealant, this ensures that the strain applied with the micrometre is the same, except little errors considered into the corrective coefficient, measured by the FBG.

The results obtained in chapter 4.2.5 shows that, if an accuracy on the temperature about 5% is enough, is possible to extend the calibration of a single FBG to all the other of the same family, that is all the FBGs with the Bragg wavelength near the one tested, without the need of a calibration of a single FBG.

In chapter 4.3.2 the results deriving from the tests shows that the thermal compensation is possible with very precise results; in this particular case, the error can be as low as two orders of magnitude below the resolution of the micrometre. Furthermore, an important thing to be highlighted is that is possible to completely bypass the temperature calculation and simply subtract the wavelength shift of the temperature FBG from the wavelength of the strain FBG; in this case the error is about three or four times greater than before but is still one order of magnitude below the resolution of the micrometre. The great advantage of not calculating the temperature is that is not necessary anymore the K_T and so is not necessary the thermal calibration of the FBG.

The work presented in this thesis will be continued by other people, so are identified some points on which the future work should focus on:

- Enhance the test device to permit the testing of the fibers directly on the item where are mounted.
- Test other kinds of glue, like cyanoacrylate, to facilitate the mounting procedure and eliminate the problems connected to the mixing of the two components of the epoxy glue.
- Perform frequency response tests to see how these innovative sensors react to vibrations at different frequencies.
- Perform thermal compensation tests using an electric micrometre to have a more accurate stressing, a defined stress history and to perform repeatability tests.

6 Appendix A – System thermodynamic model

The microcontroller used to manage the Peltier cell and presented in section 3.2 shows instability in maintaining a constant value of the temperature, especially when is required a high temperature. Moreover, the software needed to set the microcontroller has only a few settings about the PID and so the response can't be fast and in the same time accurate and without oscillations; so in a future, it will be most likely replaced with a microcontroller like Arduino.

The new microcontroller will be programmed to act like a PID with the PT100 to close the feedback loop; to find the optimal parameters that will permit to have a fast and accurate response the simple try and error on the real system is too slow, so is required a mathematical model able to simulate the response of the real system and where multiple solutions can be tried in less time; the software used are:

- Simulink to create the mathematical model.
- Matlab for the post-processing of the data.

The real configuration taken into account is the fourth layout presented in chapter 4.2.4, because it is the layout used for the thermal compensation tests.

The process used to obtain a correct model is the follow: the model is made considering certain coefficients; data are collected from the real system where is imposed not a temperature, but a constant power supplied to the Peltier cell; the model and the real data are used to find, thanks to the optimisation tool in Matlab, the values of the coefficients that fit in the best way the real response.

In Figure 6.1 is visible as an example the response of the real system to an input of 2,26 W, with the red mark is highlighted the point where the response is the 63% of the total, the time constant of the system is: $\tau = 588$ seconds, $\tau = 9$ minutes 48 seconds.

The high time constant shows the advantages of creating a mathematical model instead to try always on the real system: the model could be run with a step of 10 seconds and the entire simulation will take only a few seconds when the response of the real system will take about one hour.

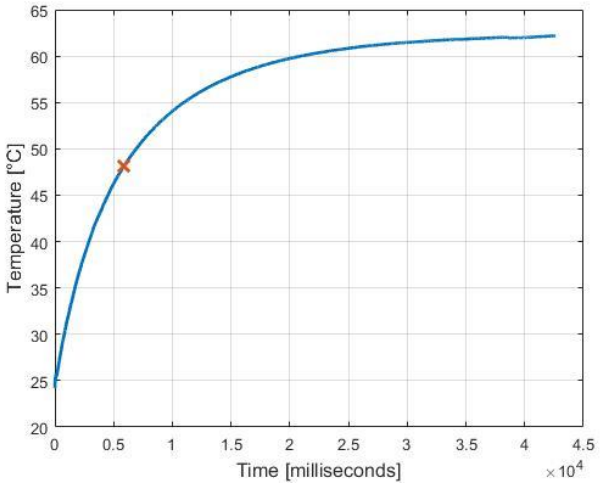

Figure 6.1: real system response to an input of 2,26 W

6.1 First order model

The first model implemented is a first order type, this try is made because a first order system would be easier and faster to run; the equation used is the following:

$$Q_{in} - Q_{out} = C_T \frac{dT}{dt} \tag{6.1}$$

The outgoing heat flow is expressed as:

$$Q_{out} = K(T - T_{amb}) \tag{6.2}$$

The parameters used are:

- C_T: is a parameter that considers the mass of the entire system and the specific heat.
- K: is a parameter that considers the heat flow from the system to the outside.

The resulting Simulink model is shown in Figure 6.2.

The values of the two coefficients are found thanks to the optimisation Matlab tool; the software compares the real response with the one of the model thanks to the least squares method implemented in a function, the aim of the optimisation tool is to find the minimum of this function.

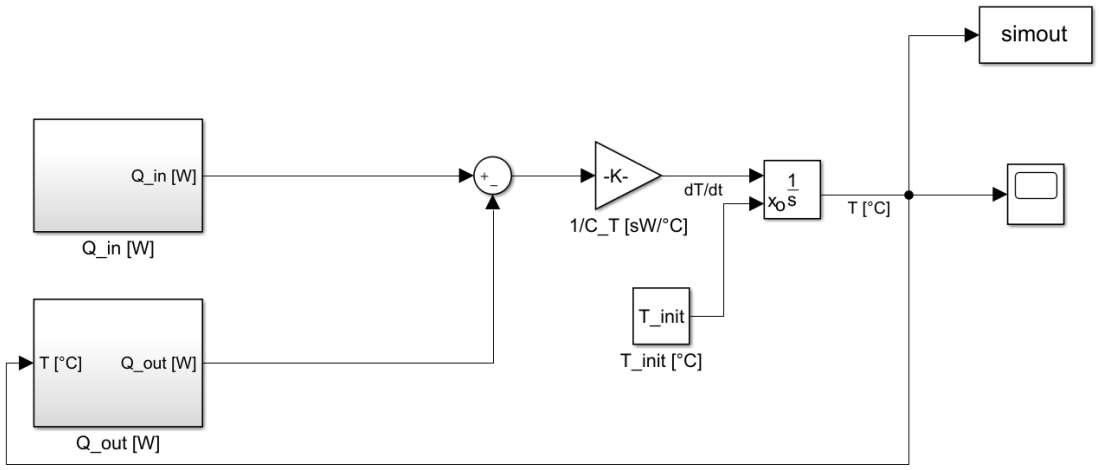

Figure 6.2: Simulink first order model

The first order model is not enough accurate to simulate the real system, as visible in Figure 6.3 the two responses are quite different: the real model has a first time when is faster in temperature increase compared to the model, then it slows down and it is the model that is faster than the real system.

These two different behaviours can be traced back to the two different elements that compose the system: the water and the PLA, the faster response is the water that is heating up, the water heating slows down when the hat start to flow consistently to the PLA.

It is necessary to switch to a second order system.

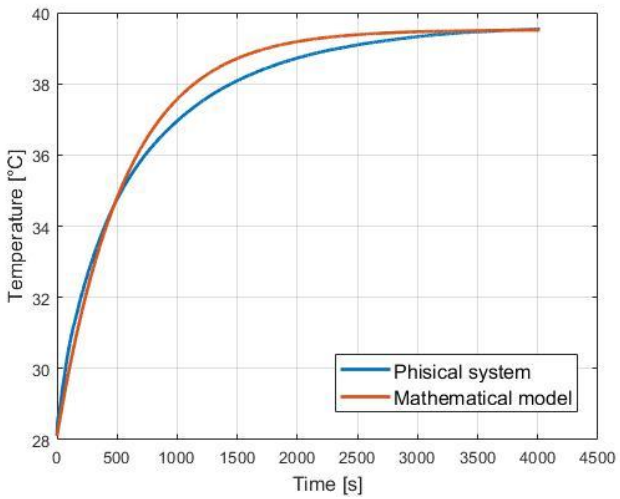

Figure 6.3: comparison between real system response and first order system response

6.2 Second order model

In the second order model, it is taken into account the heat flow from the water to the PLA and the two temperature are separate.

The starting point is the following system of equations:

$$\begin{cases} Q_{in} - Q_{H_2O-PLA} = C_{T\ H_2O} \dfrac{dT_{H_2O}}{dt} \\ Q_{H_2O-PLA} - Q_{out} = C_{T\ PLA} \dfrac{dT_{PLA}}{dt} \end{cases} \tag{6.3}$$

With:

$$Q_{H_2O-PLA} = K_{H_2O-PLA}\left(T_{H_2O} - T_{PLA}\right) \tag{6.4}$$

$$Q_{out} = K_{PLA-out}(T_{PLA} - T_{amb}) \tag{6.5}$$

The coefficients considered are now four and are the following:

- $C_{T\ H_2O}$: this parameter considers the mass of water and its thermal capacity.
- $C_{T\ PLA}$: this parameter considers the mass of PLA and its thermal capacity.
- K_{H_2O-PLA}: it considers the heat flow from the water to the PLA.
- $K_{PLA-out}$: the parameter considers the heat flow from the PLA to the outside.

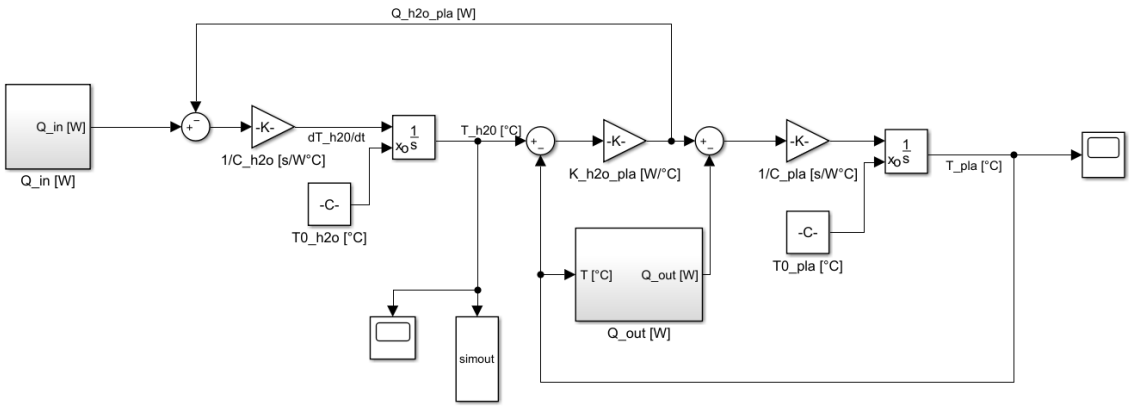

Figure 6.4: Simulink second order model

The implementation of the equations into the Simulink model is shown in Figure 6.4; to notice that the temperature sent to the Matlab Workspace to be post processed is the water one.

In Figure 6.5 is visible that the second order model is able to simulate accurately the response of the real system, both the two section with different rates of temperature variation are well reproduced.

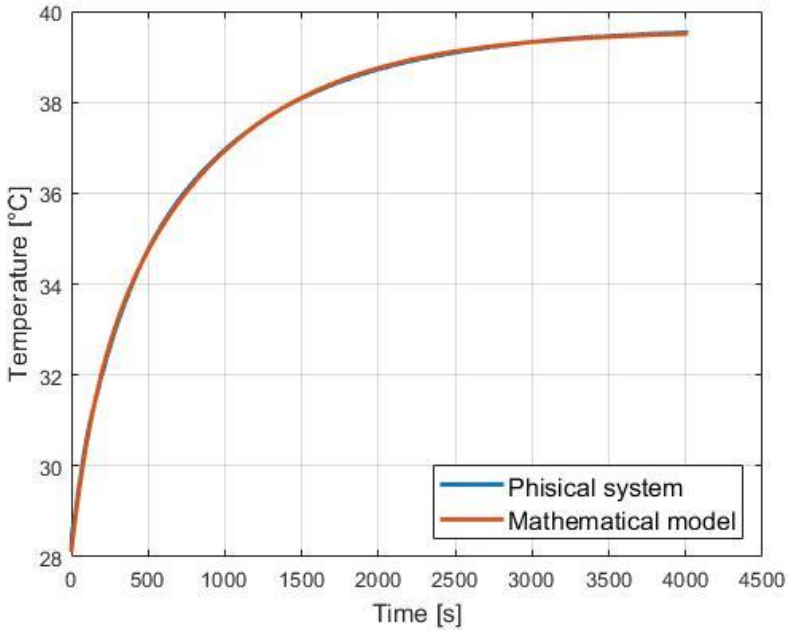

Figure 6.5: comparison between real system response and second order system response

6.3 Use of the model

Chosen the second order model for the use the four parameters are found for three different series of real system data collected in three different experiments.

The Simulink model is not used directly, but it is executed by a Matlab script; in this script the coefficients are interpolated linearly in function of the target temperature to find the value to be used; an interpolation is also used to find the power to be supplied to the Peltier to reach this temperature.

In Figure 6.6 is visible the response of the model for a desired temperature of 45°C.

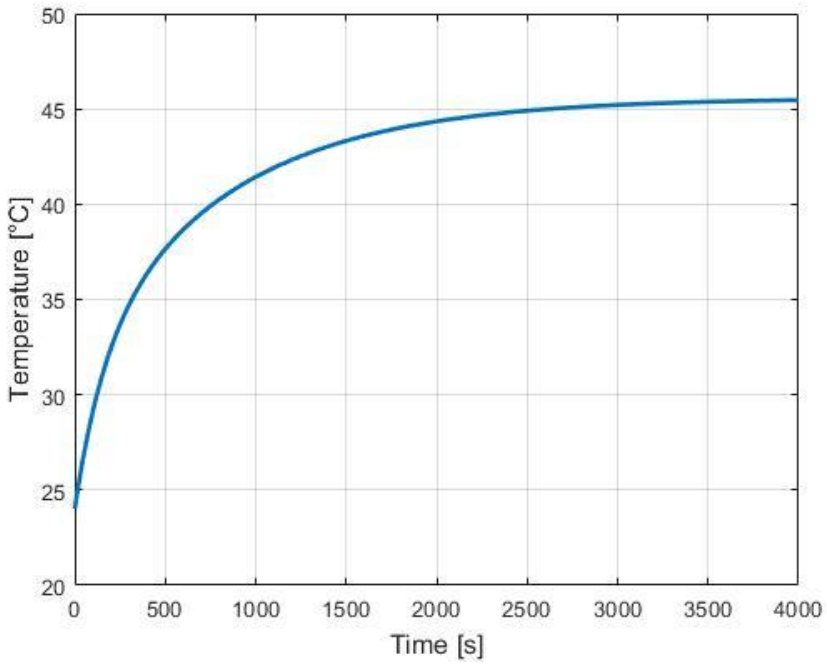

Figure 6.6: mathematical model response for an input of 45°C

The calibration of the model is made with the system placed in the office and with an outside temperature of 29 °C; when the model is placed in the laboratory with a controlled temperature constantly kept at 22 or 23 °C the response of the model changes as shown by Figure 6.7. This figure compares the response of the mathematical model and the real one, is visible a huge difference caused by the change in the outside temperature.

6.4 Conclusions

The Mathematical model developed is able to work well only if the surrounding conditions are stable; if there is a change in these conditions it must be performed a new calibration.

In conclusion, this model needs some improvements to be a starting point for future enhancement and tuning and for the implementation of the PID controller only.

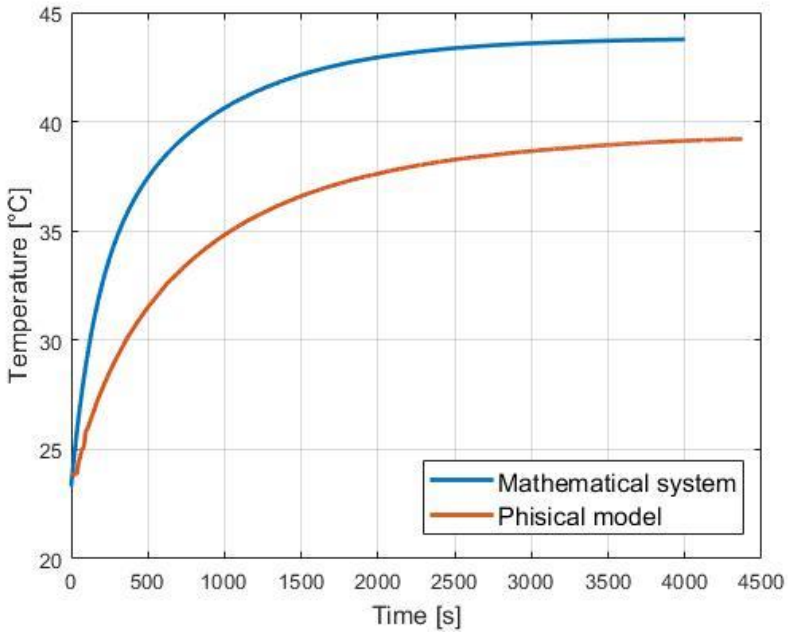

Figure 6.7: comparison between the mathematical model and the real one while the outside temperature is changed

7 References

1. *Optical sensors and their applications.* **D. Ahuja, D. Parande.** November 2012, Journal of Scientific Research and Reviews Vol. 1(5), pp. 060-068.

2. **Giurgiutiu, Victor.** Fiber-Optic Sensors. *Structural Health Monitoring of Aerospace Composites.* s.l. : Academic Press, 2016, p. 249-296.

3. *Fiber Bragg Grating Sensors for Harsh Environments.* **Mihailov, Stephen J.** 10 February 2012.

4. *A Review of Recent Developments in Fiber Optic Sensor Technology.* **Kersey, Alan D.** February 1996, OPTICAL FIBER TECHNOLOGY, p. 291-317.

5. *Temperature-compensated strain measurement.* **Tanaka, Nobuhira.** 2003.

6. *Measurements of thermo-optic coefficient of standard single mode.* **Wenyuan Wang, Yongqin Yu, Youfu Geng, Xuejin Li.** Beijing : s.n., 2015.

7. *The Good Gain method for simple experimental.* **Haugen, F.** 4, 2012, Modeling, Identification and Control, p. 141-152.

8. **Candiano, Giancarlo.** *Fiber Bragg Grating Sensors for Mechanical and Thermal Prognostics and Diagnostics for Aerospace Applications.* 2018.